AD-A080 472 BRISTOL UNIV (ENGLAND) DEPT OF AERONAUTICAL ENGINEERING F/G 20/4
PRESSURES ON A SLENDER, AXISYMMETRIC BODY AT HIGH ANGLE OF ATTA--ETC(U)
SEP 79 B L HUNT, P C DEXTER DA-ERO-77-G-073
UNCLASSIFIED NL

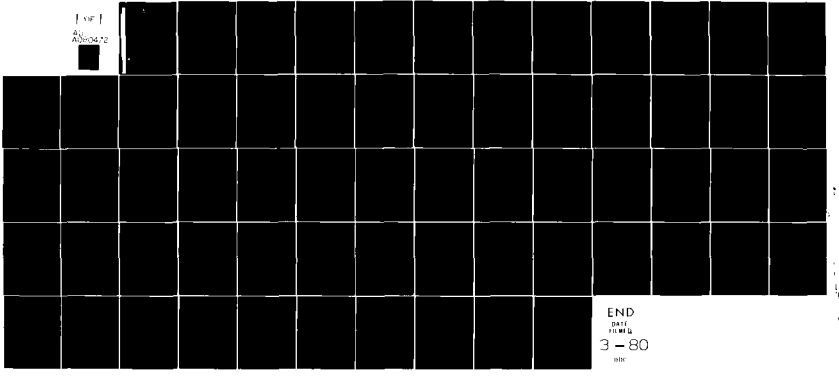

Report No. 12

UNIVERSITY OF BRISTOL

DEPARTMENT OF AERONAUTICAL ENGINEERING

PRESSURES ON A SLENDER, AXISYMMETRIC BODY AT HIGH ANGLE OF ATTACK IN A VERY LOW TURBULENCE LEVEL AIR STREAM

Second Annual Report

by

B. L. Hunt and P. C. Dexter

September 1979

U.S. ARMY EUROPEAN RESEARCH OFFICE
AND
U.S. AIR FORCE EUROPEAN OFFICE OF
AEROSPACE RESEARCH AND DEVELOPMENT
London, England
Grant Number DA-ERO-77-G-073

UNCLASSIFIED

SECURITY CLASSIFICATION OF THIS PAGE (When Data Entered)

R&D 2450

REPORT DOCUMENTATION PAGE

READ INSTRUCTIONS BEFORE COMPLETING FORM

1. REPORT NUMBER

2. GOVT ACCESSION NO.

3. RECIPIENT'S CATALOG NUMBER

4. TITLE (and Subtitle)

Pressures on a Slender, Axisymmetric Body at High Angle of Attack in a Very Low Turbulence Level Air Stream.

5. TYPE OF REPORT & PERIOD COVERED

Second Annual Report. no. 2, Oct 77 – Apr 79

6. PERFORMING ORG. REPORT NUMBER

7. AUTHOR(s)

B.L. Hunt [redacted] P.C. Dexter

8. CONTRACT OR GRANT NUMBER(s)

DAERO-77-G-073

9. PERFORMING ORGANIZATION NAME AND ADDRESS

University of Bristol
Dept. of Aeronautical Engineering

10. PROGRAM ELEMENT, PROJECT, TASK AREA & WORK UNIT NUMBERS

6 11.02A
1T61102BH57-06

11. CONTROLLING OFFICE NAME AND ADDRESS

US Army Research & Standardization Group (Eur)
Box 65
FPO NY 09510

12. REPORT DATE

Sep[redacted]79

13. NUMBER OF PAGES

59

14. MONITORING AGENCY NAME & ADDRESS (if different from Controlling Office)

16) 1T161102 BH57

15. SECURITY CLASS. (of this report)

Unclassified

15a. DECLASSIFICATION/DOWNGRADING SCHEDULE

16. DISTRIBUTION STATEMENT (of this Report)

Approved for Public Release - Distribution Unlimited

17) 06

17. DISTRIBUTION STATEMENT (of the abstract entered in Block 20, if different from Report)

18. SUPPLEMENTARY NOTES

19. KEY WORDS (Continue on reverse side if necessary and identify by block number)

High Angle of Attack;
Vortex Shedding;
Side Forces at Large Angles of Attack;
Roll Angle Dependency;
Extreme Sensitivity of Side Forces on Turbulence of External Flow.

20. ABSTRACT (Continue on reverse side if necessary and identify by block number)

The report describes the work and results of the past year on this contract to investigate the pressures on slender bodies at high incidence. Results are presented from two models used to investigate the transient nature of the pressures and from one model with two interchangeable noses used only for determining time-averaged pressures. The results show a dependence on roll angle but indicate that a regular and universal state may exist for the flow, and any other states are perturbations between the two → next page

DD FORM 1 JAN 73 1473 EDITION OF 1 NOV 65 IS OBSOLETE

UNCLASSIFIED 409 577

SECURITY CLASSIFICATION OF THIS PAGE (When Data Entered)

20. Contd.

possible hands of the regular state.

Local side force and normal force distributions are presented which show that both are affected by the vortex flow field. The investigations have largely been performed in a low speed, very low turbulence wind tunnel.

SUMMARY

The report describes the work and results of the past year on this contract to investigate the pressures on slender bodies at high incidence. Results are presented from two models used to investigate the transient nature of the pressures and from one model with two interchangeable noses used only for determining time-averaged pressures. The results show a dependence on roll angle but indicate that a regular and universal state may exist for the flow, and any other states are perturbations between the two possible hands of the regular state.

Local side force and normal force distributions are presented which show that both are affected by the vortex flow field. The investigations have largely been performed in a low speed, very low turbulence wind tunnel.

TABLE OF CONTENTS

1. INTRODUCTION

This is the second annual report as part of this contract concerning the pressures and side forces on axisymmetric bodies at high incidence and consequently an introduction into the background of this work has already been presented in the first annual report (Ref. 1). Little further is needed here except to emphasise the fact that most previous work in this field has shown that it is very difficult to achieve meaningful experimental results. The available literature shows great scatter within and between different tests, and this study is in part an attempt to resolve this position by acquiring some understanding of the important factors which have perhaps been overlooked in the past. Great care and attention have been taken over experimental details, as mentioned in Ref. 1, and some progress has been made. The two most important conclusions from Ref. 1 are that the surface pressures on a rigidly clamped model are vastly more steady in a stream of turbulence level equal to 0.01% than they are in a stream of turbulence level 0.7%, and that the surface pressures are dependent on roll angle even in the low turbulence stream.

These two conclusions alone help to explain some of the inconsistencies found in previous literature between nominally similar tests, where such fine details are possibly overlooked. In fact roll angle on an axisymmetric body has no real meaning between any two different bodies but is confined solely to the orientation of one body relative to a datum. However, no satisfactory explanation has yet been offered concerning the causes of roll angle effect and little work has been done to understand the important factors involved. It is part of this contract to try to gain this understanding and hence to establish a sensible data base.

Details of work carried out subsequent to the preparation of Ref. 1 are presented.

2. APPARATUS

The wind tunnel used for the majority of this work is the 1.2 m x 0.9 m low turbulence wind tunnel at R.A.E. Farnborough, which has a contraction ratio of 31.1:1 giving a turbulence level of about 0.01%. Additionally reference is made to some tests made in the 2.1 m x 1.5 m wind tunnel at Bristol University which has a contraction ratio of 5:1 and a turbulence level of 0.7%. Also some exploratory flow visualisation tests have been made in the 1.1 m circular open jet wind tunnel at Bristol University.

The basic model used is that as detailed in Ref. 1. It consists of a nose section with several screw-in cylindrical sections of 51 mm diameter. Two of these sections each contain 2 measuring stations which consist of 4 pairs of pressure tappings as shown in Fig. 1. In later tests a third identical section was made. Additionally there is a dummy section which can be inserted to increase the effective pressure measurement length of the model. This is fitted on to a constant diameter support body which is rigidly clamped and secured to the wind tunnel, as detailed in Ref. 1.

A second model was constructed and is shown in Fig. 2. This was made with a tight push fit between the sections instead of a screw fit and held together by rods passing through the inside of the model. This system makes it easier to obtain the correct orientation between adjoining sections. The model diameter was made 38 mm so that greater wind speeds could be used for given Reynolds numbers and hence larger pressure differences could be measured. This model was clamped in the same manner as previously. More about the model design is given later.

A third arrangement was also used. This is the model (but with new tubing) that was used in Hunt's and Lamont's work (Ref. 2) for non-transient pressure measurements at Bristol University (Fig. 3). It consists of a nose section and several screw-in sections of 51 mm diameter, each 51 mm long. Each section contains 2 measuring stations, and each measuring station consists of 36 equally spaced pressure tappings. There are 5 of these sections. These, together with the dummy section of the first model (Fig. 1), enable pressure distributions to be obtained around the model at a total of 20 stations, though 2 of these are repeats when the dummy is added,

and act as a check. This gives 18 different stations all together. This model is used to obtain the force distribution along the model, obtained by integrating the pressures.

Pressure measurement on the first two models, used for measuring transient pressures, was obtained as discussed in Ref. 1. Matched pressure transducers were backed with a suitably damped free stream static pressure and connected to tappings placed symmetrically at $\pm 75^{\circ}$ (usually) from the leading body generator, and their difference obtained electrically. The transducers were inside the body on short lengths of tube capable of transmitting pressure fluctuations of up to at least 400 Hz without significant attenuation.

The difference so obtained was passed through a galvanometer drive amplifier to a u/v recorder. The electrical circuit is shown in Fig. 4.

The system for the multi-pressure tapped model was different. The transient pressure behaviour was not needed, only the mean value being necessary. The pressure tubes used were quite long and terminated in 10 Scanivalve rings, one per model station. A data-logger system was used to drive the Scanivalve and record the pressures from a single pressure transducer. The pressure from each tube was read 3 times, after allowing a suitable settle time, and all the readings stored on paper tape. It was possible to keep a rough check on the pressures during the experiments using the u/v recorder, if necessary, as shown in the circuit diagram of Fig. 5.

3. TEST PROGRAMME

The results presented in Ref. 1 made it quite clear that even in the low turbulence flow of the R.A.E. tunnel the model being used suffered from roll angle effects. This raised several important points concerning this type of flow over inclined slender bodies, and the recent research has been directed towards them. The first aim was to try to construct a highly accurate model that shows no roll angle effect and if this could be done then to see if the pressures could be influenced in a predictable manner by minor modifications to the nose. The second aim was to see if the roll angle effect could be correlated to observable or measurable features of the model. Hence, the critical region on such body shapes for model asymmetries must be found. The third aim was to investigate the roll angle effect, to see if any evidence of change of vortex position can be observed by flow visualisation methods, and to check on the sectional side force spacing by detailed pressure measurement.

A variety of tests has been conducted with more than one model. The tests concerned with transient pressure measurement have been performed in the manner detailed in Ref. 1, and the warning concerning the slightly subjective nature of such results still applies.

4. RESULTS

4.1 High accuracy model

The previously mentioned new model was designed and constructed in order to see if the variation with roll angle could be eliminated by the use of a model of very high accuracy. The model was based on the previous design and results, but made to include more and better spacing of possible test roll angles (Fig. 2).

The previous results showed that the smoothest pressures with a large pressure difference using the model with a 3 calibre ogive nose occurred at an incidence of about 50° at a station x/D = 5 calibres from the nose tip. The pressure difference is measured as before at angles of $+75^{\circ}$ and -75° from the leading body generator. This case had been used as a'standard' case in previous tests and was chosen as the prime case for the new model. To avoid any body joins upstream of the measuring station the nose and forebody up to 5.13 calibres from the tip were manufactured in one piece. Only one measuring station was included to avoid any possible roughness effects from upstream pressure tappings. The rest of the model sections were made to join with tight push fits rather than screw fits in order to facilitate the alignment of adjoining sections. The whole model, Fig. 2, was held together by rods passing through the inside, and the model was clamped securely in support pylons as for the previous model (Ref. 1). The calibre size of the model was reduced to 38 mm, the smallest practicable, so that higher wind speeds could be used for given Reynolds numbers, and hence higher pressures would be measured. The pressure tappings were fitted at angles to give the best roll angle coverage with fewest tappings. It was planned also to be able to fit new measuring sections as required. The whole model was made in aluminium alloy in the Departmental Workshops to the highest tolerances they could achieve. When finished the model nose piece was measured on a Talyrond machine at R.A.E. Farnborough to determine the smoothness and roundness. The nose only was measured as this is considered the most important region. The results showed that the maximum departure from roundness was less than 3 microns over the entire length of the nose section, and the roughness was obviously much less than this, of the order of ½ micron maximum. See Table 1 for details. Although this is a very good finish it is probably possible to improve it by working in stainless steel rather than in the aluminium alloy, as this is too soft for a good polished finish.

The tests on the model were carried out in the manner used for the previous model. Great care was taken during tests that the model was handled only with soft leather gloves. The transient pressure difference was recorded on u/v paper and mean readings taken from it. The traces were similar in form to those obtained before with the larger model. An example is shown in Fig. 6. Testing was performed at Reynolds numbers of 0.5×10^5 and 1.0×10^5 at 50° incidence.

It was possible to test 7 different roll angles, which could be set up accurately to within a few minutes of the nominal value. The results showed that at both the lower (Fig. 7) and higher (Fig. 8) Reynolds number there was still a variation with roll angle and this was no less than it had been with the previous larger model. However, this does not mean that it is impossible to eliminate roll angle effects, as an even more precise model could probably be made, but it does show that it is a very difficult task. What was more disturbing is that certain of the results did not repeat very well although very great care had been taken in setting up the model each time. It should be said that if the model were set up and a test performed then the result would repeat very well if the test were immediately reconducted. However, if the model were disturbed, say to a different test condition, and then returned carefully to its original setting, then it may not repeat the previous result.

This immediately seems rather unfortunate but the possible reasons may be explained later by the notion of a 'regular' state and disturbances from it, particularly as the more repeatable results are for the maximum $\overline{\Delta C_D}$ values. These are of similar magnitude to the maximum values obtained with the larger model.

More tests were also performed at incidences of 40° and 60° in which the method of testing was to set up the model roll angle and leave it unchanged while tests were performed at each incidence of 40°, 50° and 60° at Reynolds numbers 0.5×10^5 and 1.0×10^5. This was done for 6 roll angles. Figures 9 and 10 show the magnitude of the measured $\overline{\Delta C_D}$ against roll angle for each incidence. It can be seen that generally the roll angle variation is of the same form for each incidence. Note that the station $x/D = 5$ is in the first half cycle of side force distribution at $\alpha = 40^\circ$ and 50° but in the second half cycle at $\alpha = 60^\circ$. The sign changes are not shown for clarity, but these occur for each incidence at the same roll angle, 150°.

This might be expected if it is the asymmetries on the model that cause the roll angle variation.

These results show that it is difficult to eliminate roll angle variations but they do not help in determining which aspect of model geometry is the cause.

4.2 58 mm Transient pressure test model

It seems very likely that the roll angle variation is caused by the model asymmetries which are somehow affecting the vortex flow field in the lee of the body. A mechanism by which this may be occurring is through the stability of the initially symmetric twin vortex system at the most upstream part of the body over the nose. If the stability of this system is highly sensitive to small changes, then perhaps the body asymmetries could be large enough to cause changes in the location of the onset of instability. This could hence lead to the vortex pattern sliding axially along the body as the roll angle varies. Due to the resultant different shedding positions of the asymmetric vortices they may also obtain different strengths, which probably means that the distribution pattern itself would change as it slides up or down the body. This shifting of the vortex pattern would be reflected in the pressure measurements made experimentally resulting in a change in the mean pressure difference $\overline{\Delta C_p}$. This has been observed already. More conclusive evidence could be obtained if the distribution of $\overline{\Delta C_p}$ is found along the body for different roll angles.

In order to achieve the necessary axial coverage two new measuring sections were made to the same design as on the original model and made to mate together so that the roll alignment is constant along the length of the body. Measurements were taken of the transient pressure difference ΔC_{op} in the manner previously described at an incidence of 50^o. Due to the time necessary to obtain readings all along the body length the tests were restricted to 2 roll angles. The zero roll datum was chosen as in previous tests this corresponded to a maximum value of $\overline{\Delta C_p}$ obtained at station x/D = 5 at 50^o incidence, and also 30^o roll was chosen because this produced the largest difference in reading from the zero roll case at the same station.

The tests covered the axial length from x/D = 4 to x/D = 9 at Reynolds numbers of 0.5×10^5 and 1.0×10^5. The mean pressure difference $\overline{\Delta C_p}$ is shown plotted in Fig. 11. It

should be noted that the side forces will not be exactly proportional to these pressure differences but are clearly related to them. It can be seen that the effect of roll angle is indeed to shift the distribution along the model, and there has been only a small effect on the amplitudes of the readings. The sign has changed. Clearly an encouraging result worthy of further investigation. Previous experimental work of Lamont and Hunt (Ref. 2) had shown that there was no shift of side force distribution with roll angle, only a change in magnitude. However, this was in a very turbulent flow.

A new testing method was devised in order to increase the speed of data collection, otherwise it would take a prohibitively long time to carry out a full test programme. Instead of mounting the pressure transducers inside the model on short lengths of tube, as had been the previous practice, the pressure tappings had long lengths of plastic tube connected to them which led outside of the wind tunnel into the observation room. The transducers were then connected across the appropriate pair of tubes as necessary. This considerably speeded up the test time as it was no longer necessary to break down the model for each station change. In fact the model remained totally intact throughout the test period, but change of roll angle and incidence were still performed from within the tunnel. This test technique limited the information available from the u/v recordings to only the mean pressure difference $\overline{\Delta C_p}$, as the tubes were too long to transmit the unsteadiness without severe attenuation. However, it was the mean values which were of most interest.

The first tests carried out in this manner were checks to verify that this system worked satisfactorily, and were repeats of the last set of transient pressure tests as mentioned above. The results, presented in Figs. 12 and 13, show good agreement. A full test series was performed covering the range of parameters as follows; incidence from 30° to 70°, 6 roll angles, Reynolds numbers from 0.5×10^5 to 1.5×10^5, 6 axial body stations. The results are presented in Figs. 14 to 22. Although there are certain obvious exceptions, the results do tend to fall into a pattern which is best shown at an incidence of 50° in Fig. 18. The main features are as follows. The distribution shows the same type of oscillating pattern as occurs for side force. The results at roll angles of 0°, 150° and 330° are virtually in perfect agreement, as is the result at 180° roll except at large distances from the nose. The distribution at 210° roll is similar in magnitude but

switched in sign, again departing at large downstream distances. At 30° roll angle the distribution is switched, shifted and differs in magnitude.

The results at other incidences are similar in nature except that the distributions at roll angles of 180°, 210° and particularly 30° may show even greater differences from the three at 0°, 150° and 330° which always agree with each other.

It seems that the flow at 0°, 150° and 330° appears to be in some kind of 'regular' state and is perturbed from it at the other roll angles, due probably to the model asymmetries. As the flow over the model nose tip is of a highly three-dimensional nature it is unlikely that small model imperfections will be having exactly the same effect over the entire incidence range, although any large imperfections probably will have significant effects throughout the range, leading to the identifiable trends detailed above.

Before these tests, and the previous set of transient pressure measurement tests, an accident happened to the model resulting in a dent near the nose tip. Using photographic techniques the nominal dimensions and position of the dent were determined and are shown in Fig. 23. Also the orientations of the dent relative to the freestream crossflow direction for each roll angle are presented. Although a convincing interpretation which will explain all the variations in the results cannot be postulated, it is worth noting that at roll angles of 0° and 330° the dent is probably downstream of the crossflow separation point and may not be affecting the flow, and at 150° roll it is symmetrically placed upstream and may be too near the leading generator to have an influence. At the other three roll angles it is more asymmetrically placed and does seem to be located at more sensitive positions. This cannot lead to a full explanation of the variation in results as it cannot explain the variations at high x/D but it does give hope that there is a prospect of obtaining reproducible results, certainly for the 'regular' state. It can be hoped that the 'regular' state is a universal one not dependent upon the model and test facility, a possibility which is worthy of investigation.

In order to assist in an investigation of this nature, it was planned to use the new 38 mm calibre model in a manner similar to these last tests, obtaining mean pressure differences through long lengths of tubing. Unfortunately, the Departmental

Workshops made a poor job of adding the necessary extra pressure tappings, with the result that the surface became marked near the tappings to such an extent that it was decided better not to continue with the tests at that time. Fortunately the model nose region remained unscathed, so it may be possible to conduct the tests at a later date if desirable, and if it can be shown that the marks will have little effect on the results.

4.3 Multi-pressure tapped model

Following on from the results obtained for a mean pressure difference across the body it became clear that there may be a 'regular' state for the flow, and this state should be investigated more fully. In order to do so a multi-pressure tapped body has been used. This is the same body as that used by Lamont and Hunt (Ref. 2) in earlier work in the Bristol University wind tunnel. The model consists of a nose section plus five screw-on measuring sections. Each 50 mm calibre measuring section has 2 stations of 36 pressure tappings. By using a suitable dummy section it is possible to obtain readings at 18 different stations plus 2 repeat stations at the body/dummy junction, as shown in Fig. 3. New pressure tubing was fitted to the model that would reach out of the wind tunnel into the observation room and allow mean pressure values to be obtained via a Scanivalve and data-logger system.

In order to ensure that the model nose roll alignment remains constant with or without the dummy section in place, it was necessary to manufacture a new dummy section in the Workshops. Unfortunately while the screw fit was being accurately made the nose tip was damaged and subsequently had to be reformed. This obviously makes it impossible to relate directly any previous results to those obtained in subsequent tests, except for the 'regular' state.

Additionally, in order to check upon the validity of a universal 'regular' state, a new nose was manufactured out of stainless steel to the same specification, i.e. a 3 calibre tangent ogive nose. Comparison of results between the two noses may determine if there is indeed a universal 'regular' state.

The nature of the testing is such that each test takes a long time, restricting the number of results which have so far been obtained. The pressures can be checked to a certain

extent during the testing, but the readings themselves have to be processed by computer at Bristol. Each pressure is read three times and the average value calculated. These are converted into pressure coefficients, and then plotted by computer. Inspection of the plots reveals any erroneous readings, for example due to pressure tubes blocked or such like. Readings are then corrected and fed into a second program which integrates the circumferential pressure distributions and produces the side force and normal force coefficients based on cross-flow dynamic head at each measuring station. Note that usually less than 1% of the readings are in error.

The testing so far has covered, apart from the initial setting up test at 90° incidence, only one incidence angle, 50°, and roll angles of 0°, 30°, 60° and 90° at a Reynolds number 1.0×10^{5} for both noses. The results are shown as side force and normal force distributions in Figs. 24 to 31.

The first point to note is the good agreement at stations $x/D = 7\frac{1}{2}$ and $x/D = 8$ (in all cases) where the readings are measured first with the nose section attached to the measuring sections and then repeated with the dummy section in place. This shows that the addition of the dummy did not affect the flow significantly.

The next and most important feature is the excellent agreement shown between certain of the results.

Considering firstly the side force distribution it can be seen that the curves for the old nose at roll angles of 0° and 30° (Figs. 24 and 26) and the steel nose at $\Phi = 0^{\circ}$ (Fig. 25) are almost identical, and the old nose at $\Phi = 90^{\circ}$ (Fig. 30) shows excellent agreement except that the curve is inverted, corresponding to an exactly switched state. The other curves do not correspond to these or any pair to one another. It is also noticeable that the greatest local side force, presumably corresponding to the strongest vortex pattern, occurs for the cases which are in agreement.

These results obviously lead to the conclusion that there will indeed be a 'regular' state for the flow, which may be of either hand as the sign of the output has little significance, and the 'regular' state will be universal for all bodies of the same specification. Other vortex flow patterns are possible but these are present only as disturbances from the 'regular' state, generally when the body is at a roll orientation

corresponding to a position between the 'regular' state of one hand and the other. This is illustrated in Fig. 32 where the maximum local side force coefficient has been plotted against roll angle for each nose and shows the trend indicated above. The non-regular states correspond to a change in both strength and position of the associated vortices, as previously postulated. The position of the start of the asymmetry in the flow is produced at different axial stations leading to the asymmetric vortices being shed at different stations, and with different strengths.

If the value of local side force coefficient is related directly to asymmetric vortex strength, and as yet this is not clear, then the stronger the first asymmetric vortex the earlier it is shed. This is illustrated in Fig. 33 where the value of the maximum local side force coefficient in the first half-cycle of the distribution is plotted against the axial station of the first node point, for all tests from both noses.

The 'regular' state is likely to be the one of most importance to the project engineer as it involves the largest forces. It is notable that in the particular cases tested the least perfect of the two noses, the old nose, tends most toward the 'regular' state. This is very encouraging because, although these are limited data which do not indicate that the old nose will necessarily show the greatest overall tendency towards the 'regular' state, it does mean that even imperfect models can be used in wind tunnel tests and still effective results can be obtained, providing the tests are carried out properly and carefully.

More evidence of a universal 'regular' state can be provided by comparison of the transient pressure difference results on the two models used. At 50^{o} incidence there is a tendency for the most repeatable results for a given roll angle on the 38 mm model (Figs. 7 and 8) to be those providing the largest output, indicative of the strongest vortex pattern. The output was generally at or near the largest for most roll angles, and the largest value, $\overline{\Delta C_p} \approx 2.2$, is also the largest value obtained with the 51 mm model under the same conditions (see, for example, Ref. 1, Figs. 17, 18 and 24). If these are corresponding to the 'regular' state then they indicate a universal result.

The local normal force coefficient distribution is also shown in Figs. 24 to 31. In the cases corresponding to the

'regular' state the normal force distributions also agree very well. It can be seen that the asymmetric vortex pattern does have an effect on the normal force though it is difficult to ascertain this effect precisely. However, it can be seen that when there is a strong vortex pattern the local normal force coefficient is high, and reduces down to a more usual value associated with crossflow laminar drag when the vortex pattern is weak. This is true both for cases where there is never a strong vortex pattern, e.g. Fig. 28, or where the pattern is strong at upstream stations but grows weaker at downstream stations, as in the majority of the cases. This has probably not been appreciated before by most experimenters. These normal force distributions also add credence to the notion of a universal 'regular' state.

It will be interesting to see what results are achieved in future tests. It is planned to introduce some new equipment to speed up data acquisition before any more tests are undertaken but clearly many more tests covering a much greater range of parameters are necessary before these conclusions can be fully justified but it opens up an exciting possibility. If it can be shown that there is a 'regular' state which is universal for all similar models then many of the problems previously associated with high incidence aerodynamics can be overcome, by ensuring that tests are always carried out in this 'regular' state. This may involve more testing than was previously necessary to ensure that measurements will be taken in this state but it does then mean that the results achieved will have a universal significance, not confined solely to the model under test. This would also help to explain why the previous literature available on high incidence aerodynamics contains so many anomalies. If tests have been performed at arbitrary roll angles then the results are likely to be just as arbitrary. In future, tests could be performed correctly and a whole new set of data collected on effects of such things as nose bluntness, Mach number, Reynolds number, turbulence, etc. These would correspond to the 'regular' state which is probably the case the designer or project engineer is most interested in.

5. ADDITIONAL WORK

5.1 Flow visualisation

During this period work has also been progressing at a low priority on suitable methods of flow visualisation. This has largely involved testing in the Bristol University 1.1 m circular open jet wind tunnel. While this facility is not suitable for obtaining final results due to its small size and poor flow quality it is very convenient and easy to use and provides a good means of developing flow visualisation methods.

It is hoped that by finding suitable techniques it will be possible to relate the flow field structure to the pressures and forces developed on the body. Although it is obvious that the alternating pressures and forces along an inclined body are dependent on the vortex shedding many of the details are still unknown.

Several methods of visualisation have been tried with differing success.

5.1.1 Smoke and helium bubbles

Both methods involve a means of injecting something into the flow upstream of the model. This immediately causes a problem in itself, as the presence of a probe or other injector upstream of the model will add turbulence to the flow over the model. Also the helium bubbles impinge on the model and coat it in soap solution. It has also been found that at test speeds corresponding to the Reynolds numbers used in the pressure tests more smoke is required than can be produced. The helium bubbles are better in this respect although care must be taken in lighting the bubbles correctly and adequately. It is found that photographing the bubbles gives the best results if the shutter speed is fairly slow to produce streak lines from the bubbles.

Placing the injector into the flow in the lee of the body overcomes the problem of causing upstream turbulence, but poses the problem of what effect it may be having on the lee flow, and also does not show so much flow detail. More about this later.

5.1.2 Spinners

Spinners have been used to track the vortex cores behind

the body fairly successfully. However, they have drawbacks in that their position cannot be readily determined and they give no indication of the steadiness of the flow pattern. Additionally it is hard to tell if some of the flow details have been omitted, and it is impossible to get very close to the body. They may also be affecting the flow.

5.1.3 Wool tuft probes

Wool tuft probes have been tried. The same comments apply as for spinners except that it is possible to probe closer to the body.

A wool tuft probe was tried in the wind tunnel at R.A.E. Farnborough, not in a particularly scientific manner, but whilst it was possible to observe simultaneously the pressure difference ΔC_p. This showed that for the majority of positions downstream of the body the probe had no effect on ΔC_p, unless very close to the nose tip region. Further downstream, even ahead of the pressure ports, it had no noticeable effect on the pressures. It was possible to locate approximately the attached body vortices along the body length, and these are sketched in Fig. 34 for the 38 mm calibre body at incidence 50° and Reynolds number 0.5×10^5 for two different roll angles. Note the different patterns, resulting in different measured ΔC_p values.

The fact that this probe could be placed in the vortex flow field is encouraging.

5.1.4 Wool tuft grids

In view of this result it may be possible to use wool tuft grids in the flow in the lee of the body, recording the results photographically. As there seems to be very little information available on the design or relative dimensions of wool tuft grids a limited study has been conducted. This involved the construction of four small grids each 12 cm square and mounted on handles about 1 m long. Each grid was constructed of fine wire, the differing mesh sizes being 1.0 cm, 1.5 cm 2.0 cm and 3.0 cm. At the wire crossover points the wool tufts were attached, each tuft being the same length as the grid size. These grids were then held behind the inclined body in the flow of the open jet wind tunnel. It immediately became obvious that the tufts were not pliant enough, so they

were redesigned. Instead of being attached directly to the wire the tufts were connected to fine pieces of cotton of length 1 cm, which were in turn attached to the wire grid crossovers. This design, as expected, proved much better. It then became a choice of the most appropriate grid size and tuft size. The 1.5 cm size seems about the optimum to show up the flow features, although none have been tested whilst the model surface pressures were being monitored. This must be done in order to detect any interference the grid may be having on the flow. A larger area, better constructed and mounted grid would be used for proper tests if these results prove promising.

Problems associated with all the above techniques are mounting of appropriate lighting and cameras in the R.A.E. wind tunnel, which would be more difficult than in the Bristol University open jet wind tunnel where there is free access all around the working section.

5.1.5 Surface flow

Some tests have been carried out in the open jet wind tunnel to develop this technique and some encouraging results have been obtained. On a model comprising a nose section, a dummy section and the support body some very detailed surface flow patterns have been produced using Day-Glo pigment in paraffin with a very small quantity of Oleic acid. The major problems associated with this method are as follows. The body surface is no longer the same as it was without the oil film. This, of course, can have a major effect on the flow that develops, so it will be necessary to monitor the surface pressures simultaneously. However, the oil may well run into the pressure tappings and block them, unless the body is only partially covered resulting in a limited area of visualisation. This may be practical, but would be of most use provided the pressures over the body are not altered by the oil coating. Interpretation of the surface flow patterns can be very complex, judging from preliminary results. It may well prove quite difficult to correlate the flow patterns to the measured surface pressures for a given flow condition, and also to determine the larger flow features in the lee of the body.

However, if the technique can be made to work satisfactorily it will be well worth doing as it can be used at proper test speeds easily. The method developed at Bristol can easily be used at R.A.E. as no special lighting is required

actually on the model during the tests. The results can be recorded photographically quite easily and well, preferably using ultraviolet illumination in a dark room, as the Day-glo pigment shows up well in this manner.

5.2 Wind tunnel constraint

One problem associated with any wind tunnel testing is the effect of the constraint of the wind tunnel walls on the flow. This can manifest itself in a number of ways depending on the particular tests being performed. In the experiments performed in this study it is thought that the primary problems will be concerned with lift interference and blockage.

5.2.1 Lift interference

In wind tunnel lift interference the wall constraints effectively produce a change in incidence at the model. The amount of the change is related to the lift developed by the body and the proximity of the walls. With small models the total model lift can be used to calculate the change, but with longer models the incidence change will vary along the body length effectively producing a curvature in the streamlines. The amount of incidence change can be calculated by relating the lift developed to vortex strength. The vortex produces images in the walls, and these cause the incidence change. Of course, the images themselves produce images and so on ad infinitum, although the more distant reflections have very little effect on the flow in the wind tunnel. This can be modelled mathematically and Garner in Ref. 3 gives an expression that might be used for finding the induced upwash velocity for long slender models in rectangular tunnels. The lift distribution is represented by a series of point lifts and then the downwash can be calculated at any given point from the following expression:-

$$\frac{w_i}{U} = \sum_N \frac{L_N}{\rho U^2 b^2} \left\{ \frac{-b^2}{4\pi} \frac{\partial}{\partial y} \left[W\left(\frac{x - x_N}{\beta}, y - y_N, z - z_N \right) \right] \right.$$

$$+ W_c\left(\frac{x - x_N}{\beta b}, \frac{y - y_N}{b}, \frac{z - z_N}{b} \right) - W_c\left(\frac{x - x_N}{\beta b}, \frac{y - y_N}{b}, \right.$$

$$\left. \frac{z - h + z_N}{\beta b} \right) + W_c\left(\frac{x - x_N}{\beta b}, \frac{y - b + y_N}{b}, \frac{z - z_N}{b} \right)$$

$$\left. - W_c\left(\frac{x - x_N}{\beta b}, \frac{y - b + y_N}{b}, \frac{z - h + z_N}{b} \right) \right\} \qquad \text{(Eqn.1)}$$

where

$$W_c\left(\frac{x}{b}, \frac{y}{b}, \frac{z}{b}\right) = \frac{b^2}{4\pi} \sum_{-\infty}^{\infty} \Sigma \frac{\partial}{\partial y} \left[W\,(x,\ 2 - mb,\ z - 2nh)\right] \quad \text{(Eqn.2)}$$

where

$$\frac{\partial}{\partial y} W(x,y,z) = \frac{y^2 - z^2}{y^2 + z^2} + \frac{x\left[(y^2+z^2)(x^2+y^2-2z^2) - 2x^2z^2\right]}{(y^2+z^2)^2\ (x^2+y^2+z^2)^{3/2}} \quad \text{(Eqn.3)}$$

This is obviously a very complicated expression so a computer program was written to perform the calculation. The expression involves the summation of terms from $-\infty$ to $+\infty$, for strict accuracy, but this is impractical. Instead the calculation was performed several times with the number of summations increasing each time until the resultant answer varies only slowly with each increase. The equations give the resultant overall downwash due to the primary vortex system and its images. In calculating the effect of the wind tunnel wall constraints only the downwash due to the images need be included, so the first part of the expression

$$W\left(\frac{x - x_N}{\beta},\ y - y_N,\ z - z_N\right)$$

can be excluded.

Some exploratory calculations have been performed making some assumptions about the lift and its distribution based on results obtained by Lamont and Hunt (Ref. 2). The case chosen was 50° incidence and the calculations performed for the planes containing the lift and the side force. This was considered one of the worst cases as large forces are developed on the body at large distances from the tunnel centreline, and also there is a reasonable amount of available data to work from. In both planes it was found that summations from -4 to +4 representing 4 image sets from each pair of walls was well adequate for the calculation. The change in incidence at the selected points along the body for which the calculations were performed was quite small, of the order of 0.1°. This showed that in fact it is probably not worth attempting to correct the results for change of incidence due to lift interference, although for correctness and completeness a fuller investigation will be undertaken at a later date.

5.2.2 Blockage effects

Blockage effects arise in wind tunnel testing because the walls constrain the air to flow through a smaller cross-sectional area than it would if the constraints were not there. This is because both the model and its wake occupy some of the available area, so the air is forced to increase in speed through the smaller gap, and it is also possible that the position of flow separation points may be affected. (It has been shown (Ref. 4) that even for quite high blockages the separation points on circular cylinders do not vary.) The dominant effect is usually taken to be a simple increase in freestream velocity related to the volume distribution of both the body and the wake.

Standard methods can be used for calculating both the body and wake blockage if there is essentially streamline flow, or Maskell (Ref. 5) provides a method suitable for bluff body flow.

However, the current tests seem to fall somewhere between the two and make the estimation of blockage effect difficult. The calculation is also complicated by the presence of quite large model support struts being placed in the flow behind the model. Inviscid calculations show that the struts would normally have very little effect on the unconstrained flow over the body, but it may have a blockage effect due to the wall constraints.

Several methods have been studied including those of Maskell (Ref. 3), Fackrell (Ref. 6) and Peitzman (Ref. 7), but no conclusions can yet be made concerning the size of any blockage effects or corrections which ought to be made. This is still a matter of continuing study, but it is felt that even if the correction terms are moderately large it will not affect the basic research which is being undertaken.

6. PUBLICATIONS

The authors presented a paper at the AGAPL FDP Symposium on high incidence aerodynamics held in Sandefjord, Norway, in the period 4th - 6th October, 1978. The paper was based on work carried out under this contract and has appeared in the conference proceedings, Ref. 8.

7. CONCLUSIONS

The main conclusion to be drawn from this work is that results are dependent on roll angle but that there might exist a 'regular' state for the flow and other states are perturbations from this. In any complete roll traverse the flow would tend to remain in the 'regular' state or its switched condition, or otherwise would be in some intermediate state between the two. In the non-regular states the associated vortices are of a different strength and position. This is consistent with the notion that the roll angle dependence is produced by small disturbances affecting the stability of the two initial nose vortices and subsequent growth of asymmetry. It is the 'regular' state which produces the largest forces, and the 'regular' state will probably be universal, i.e. any models of similar geometry will have the same 'regular' state. This is an important conclusion as it means that as long as tests are performed in this 'regular' state they should always be reproducible. It was also found that the pressures on two different sized similar models were similar, which is further evidence of a universal regular state. A result of these conclusions is that future tests, which must be done to verify the results obtained and to expand the range of the data collected, can be conducted meaningfully and properly.

Information obtained showed that the local normal force varied with the strength of the vortex flow field. When there is a strong vortex flow field present the local normal force coefficient is high, reducing to a more usually accepted level when the vortices are weaker. This has not been observed before.

8. REFERENCES

1. Hunt, B.L., Dexter, P.C. Pressures on a slender axisymmetric body at high angle of attack in a very low turbulence level air stream. University of Bristol, Aero. Eng. Dept. BLH/7801, 1978.

2. Lamont, P.J., Hunt, B.L. Pressure and force distributions on a sharp-nosed circular cylinder at large angles of inclination to a uniform subsonic stream. J.F.M. Vol. 76, Part 3, pp. 519-559, 1976.

3. Garner, H.C. Lift interference on three-dimensional wings. Chapter 3, AGARDograph 109, 1966.

4. Modei, V.J., El Sherbiny, S. On the wall confinement effects in industrial aerodynamic studies. Paper 116 at Symposium on Vibration Problems in Industry, held at Keswick, England, 1973.

6. Fackrell, J.E. Blockage effects on two-dimensional bluff-body flow. Aero. Quart., 26, 4, 243-253, 1975.

7. Peitzman, F.W. Determination of high attitude wall corrections in a low speed wind tunnel. AIAA Paper 78-810, 1978.

8. High angle of attack aerodynamics (Paper 17), AGARD-CP-247, 1979.

9. NOTATION

ΔC_p Coefficient of pressure difference between points equidistant from leading body generator, based on crossflow dynamic head

$\overline{\Delta C_p}$ Mean value of ΔC_p

C_n Local normal force coefficient based on crossflow dynamic head

C_y Local side force coefficient based on crossflow dynamic head

D Diameter of body (= 1 calibre)

R_{max} Maximum body radius at given axial station

R_{min} Minimum body radius at given axial station

Re Reynolds number based on $D/\sin\alpha$

α Angle of incidence

θ Angular position relative to leading body generator

ϕ Roll angle

In equations 1, 2 and 3

b Breadth of wind tunnel

h Height of wind tunnel

L_N Point concentration of lift

m Integer defining column of vortex images $y = mb$

n Integer defining row of vortex images $z = nh$

U Velocity of undisturbed stream

w' Upwash function relating to horseshoe vortex.

W_c Upwash function

w_i Interference upwash velocity

x Streamwise distance

y Spanwise distance from centre of tunnel

z Upward distance from centre of tunnel

Subscript

N Refers to point concentration of lift

mm FROM NOSE TIP	$R_{max} - R_{min}$ μm	$\theta^{\circ}_{R_{max}}$	$\theta^{\circ}_{R_{min}}$
5	2·6	106	214
10	2·4	107	211
15	1·8	98	189
20	2·4	110	182
25	2·8	97	192
30	2·6	101	198
35	2·8	93	189
40	2·0	252	193
50	2·0	247	200
60	2·0	106	42

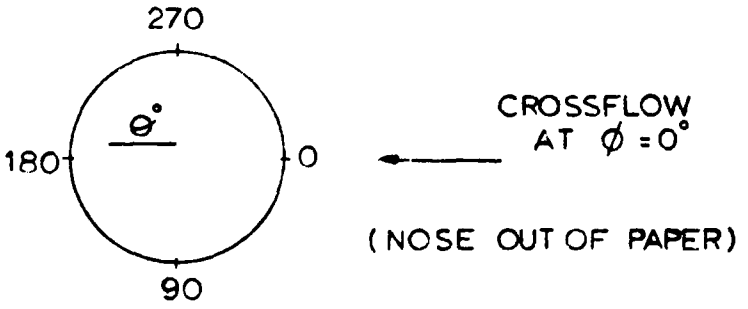

TABLE 1 38 mm MODEL NOSE DETAILS

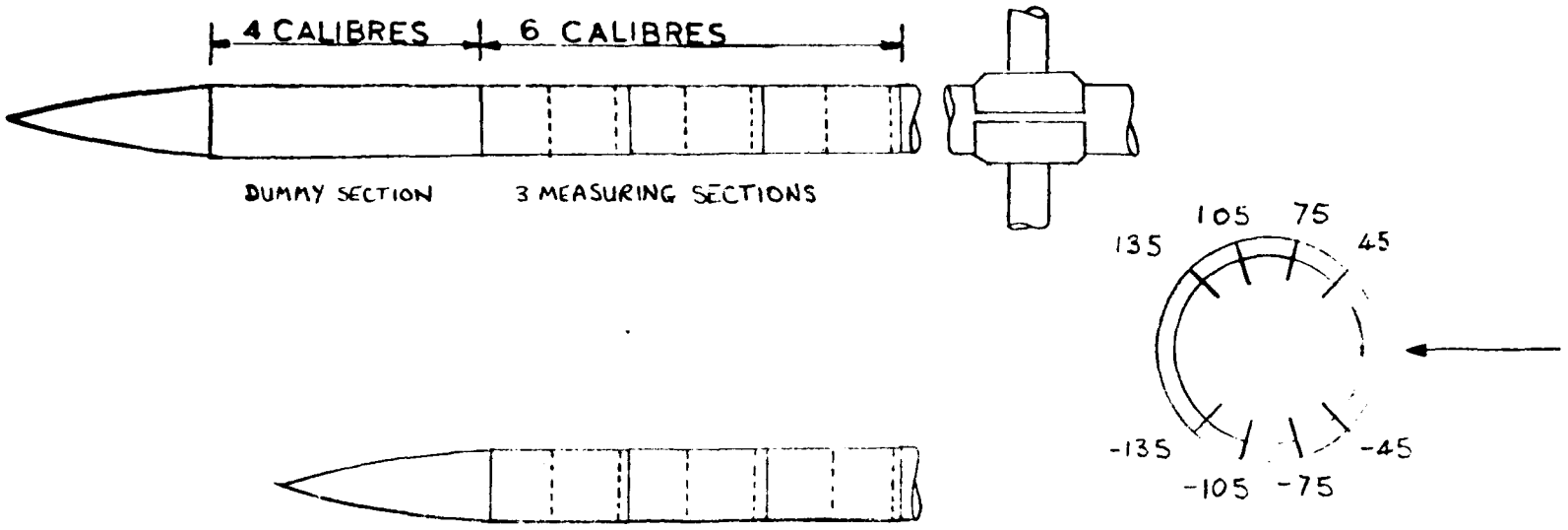

FIGURE 1 51 mm TRANSIENT PRESSURE TEST MODEL

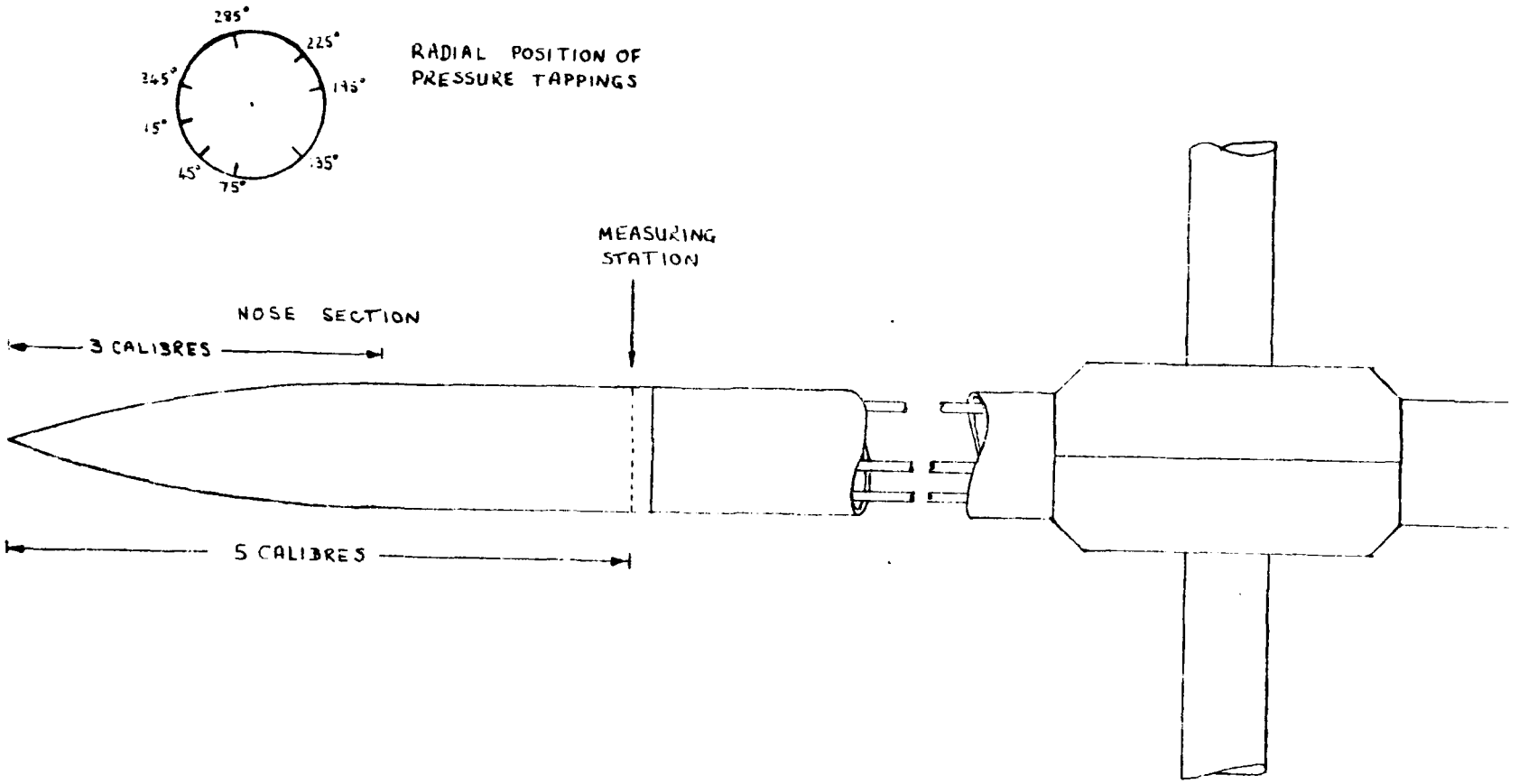

FIGURE 2 38mm TRANSIENT PRESSURE TEST MODEL

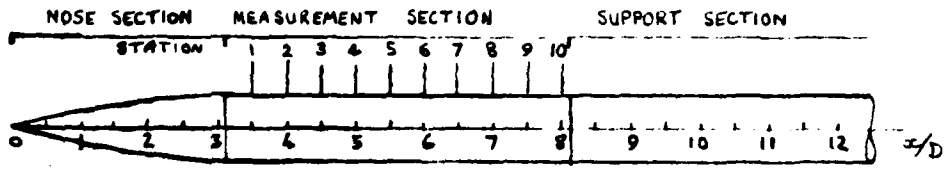

MEASUREMENT SECTION IN FORWARD POSITION

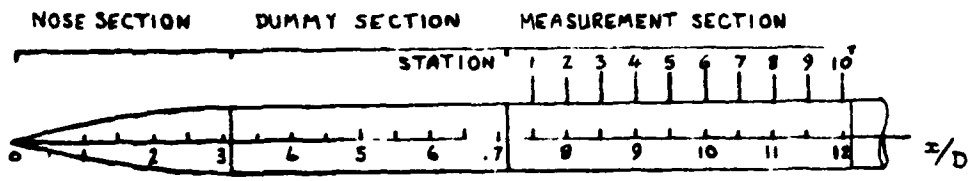

MEASUREMENT SECTION IN REARWARD POSITION

FIGURE 3 MULTI-PRESSURE TAPPED MODEL

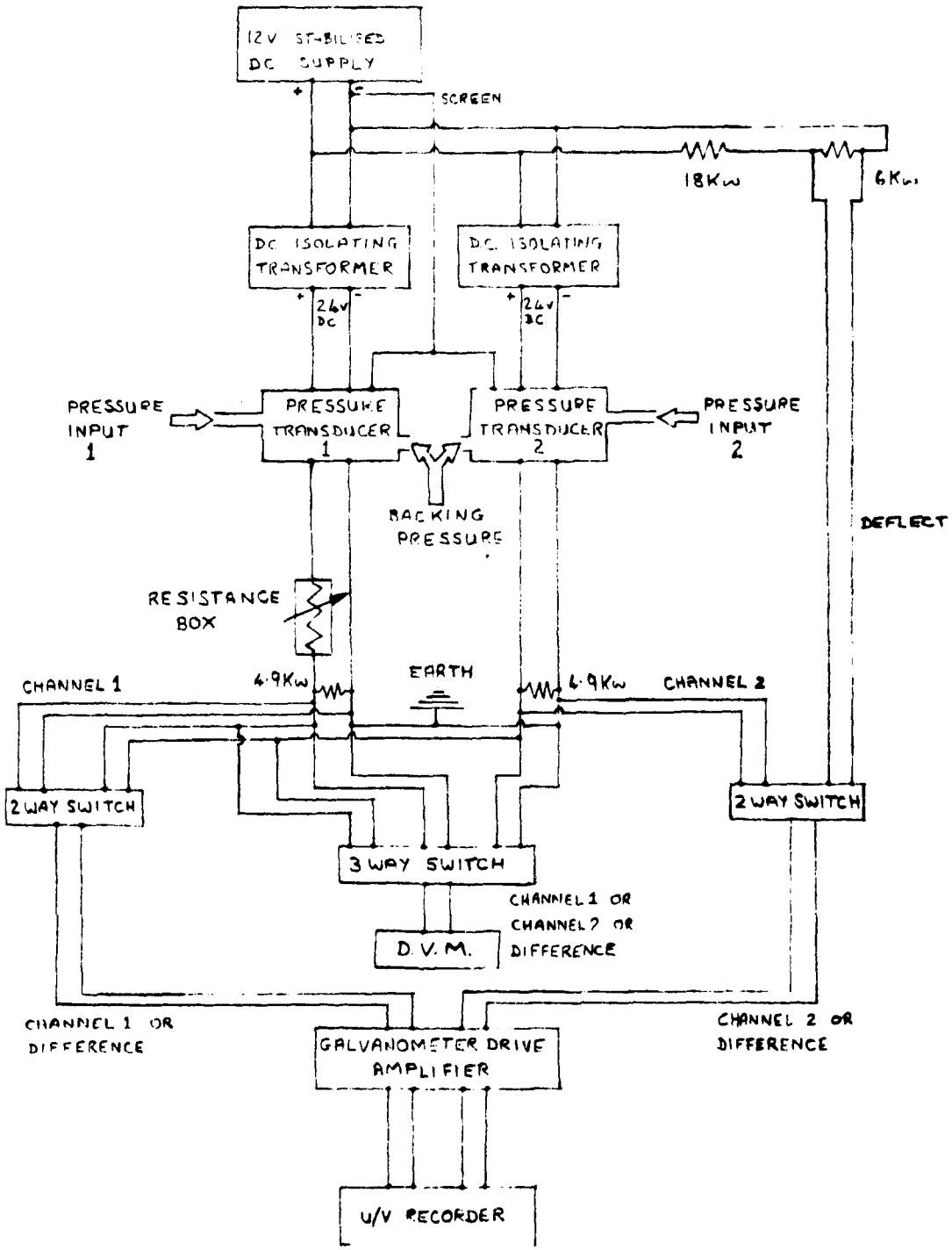

FIGURE 4 TRANSIENT PRESSURE RECORDING SYSTEM

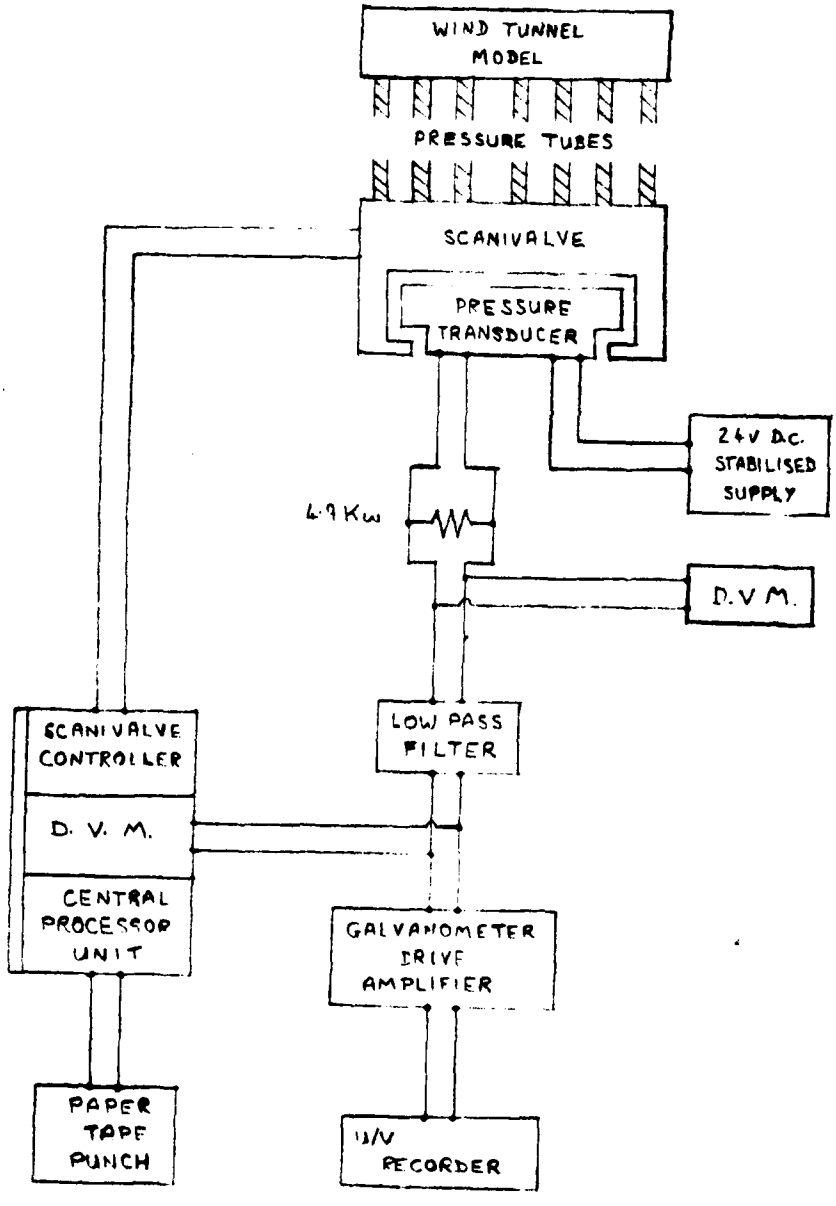

FIGURE 5 MEAN PRESSURE RECORDING SYSTEM

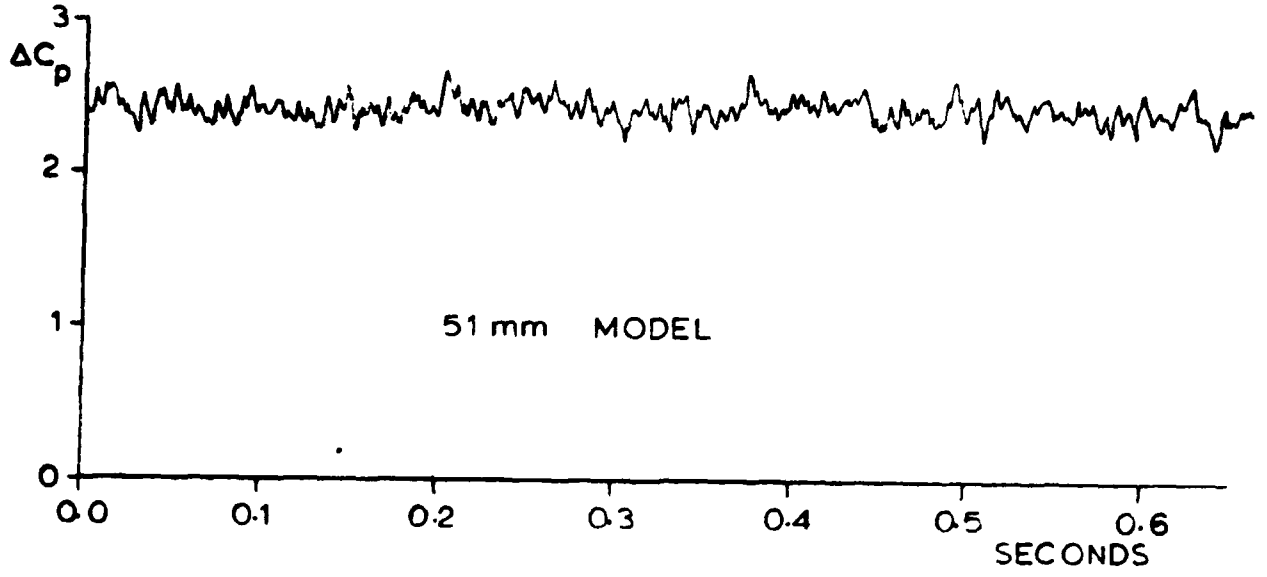

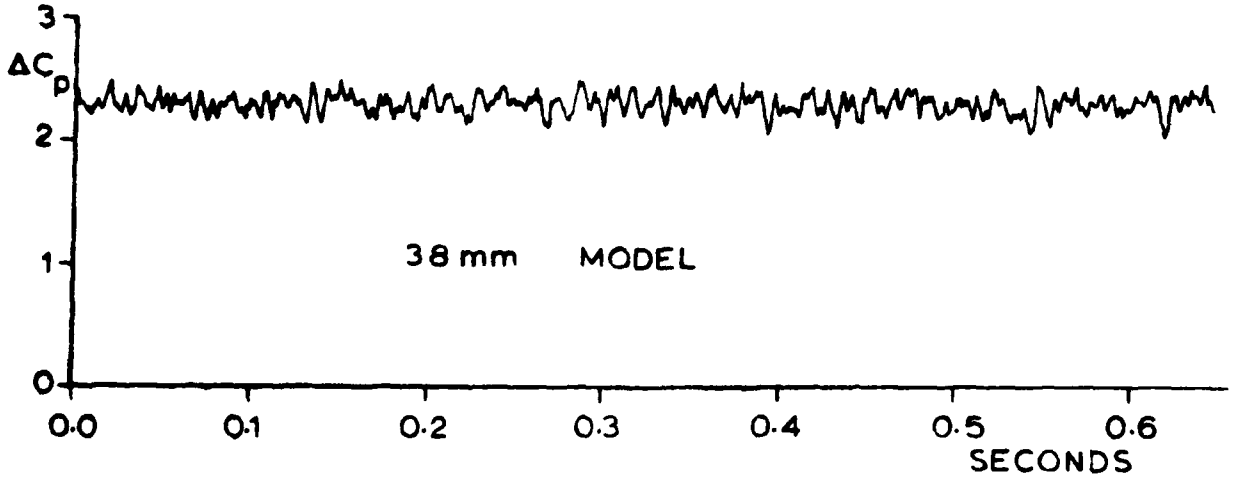

COMPARISON OF PRESSURE TRACES

$\alpha = 50^\circ$, $x/D = 5$

FIGURE 6

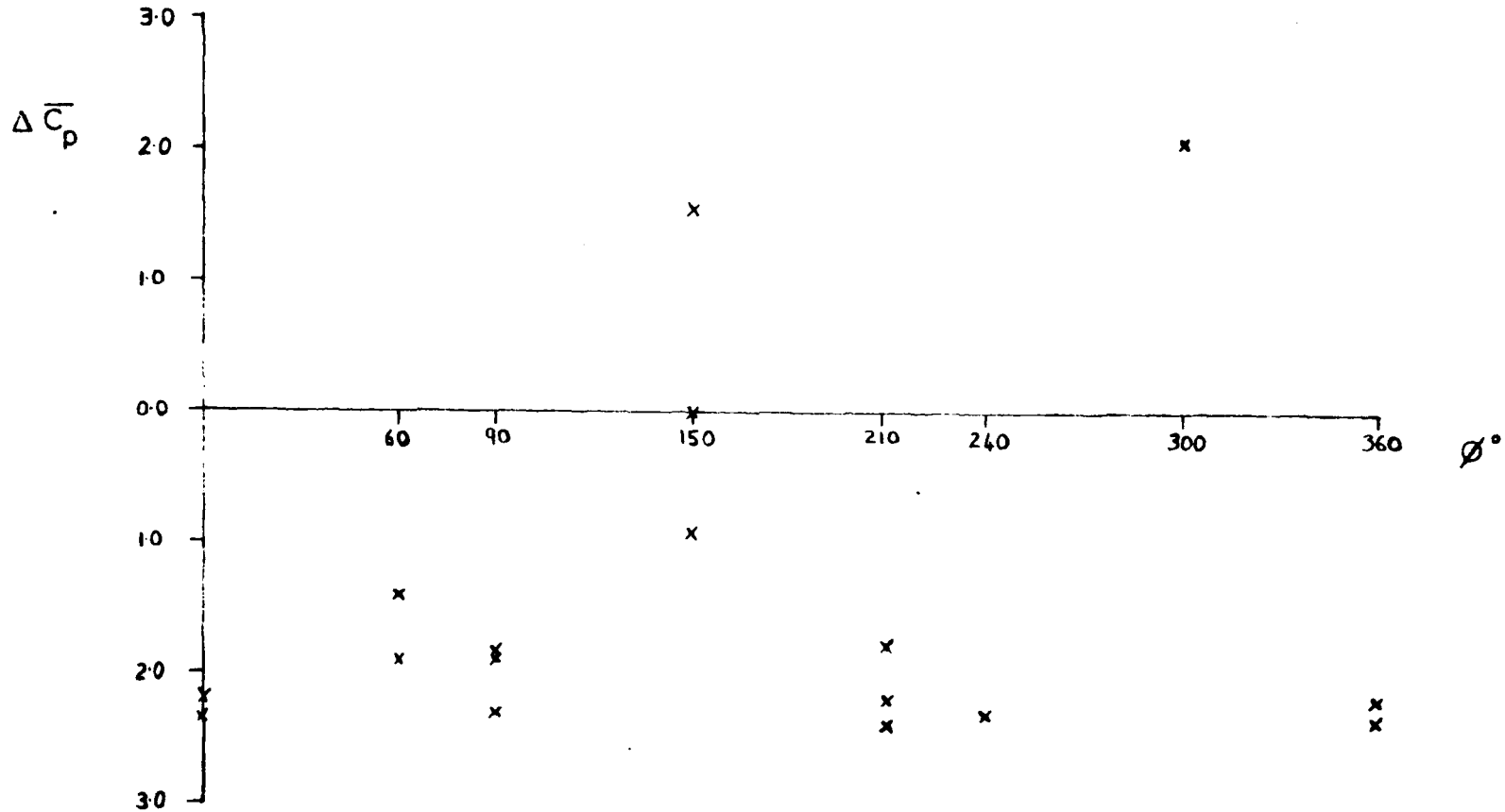

FIGURE 7 VARIATION OF MEAN ΔC_p WITH ROLL ANGLE ON 38mm MODEL
$\alpha = 50°$, REYNOLDS NUMBER 0·5E5, $x/D = 5$

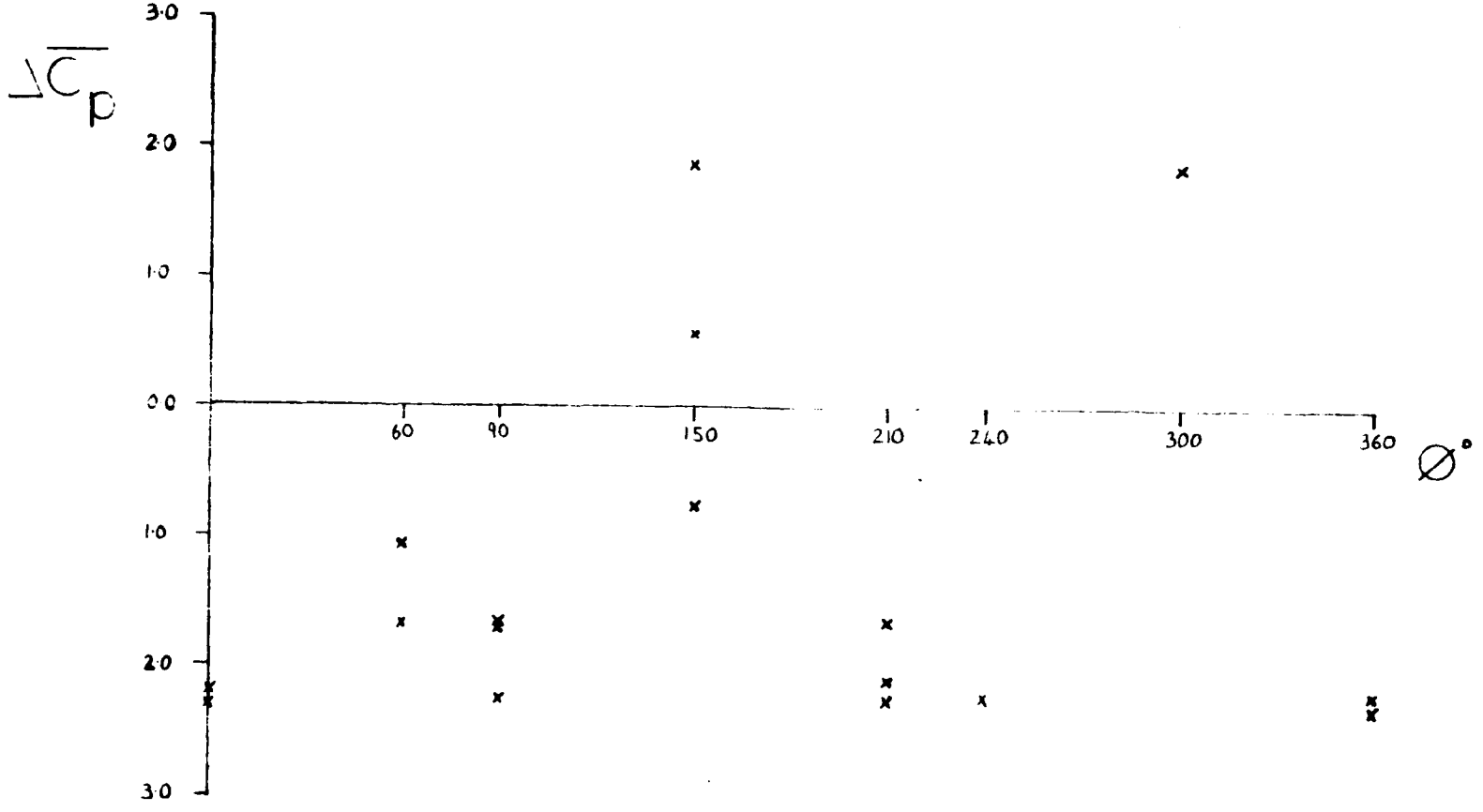

FIGURE 8 VARIATION OF MEAN ΔC_p WITH ROLL ANGLE ON 38 mm MODEL

$\alpha = 50°$, REYNOLDS NUMBER 1·0E5, x/D=5

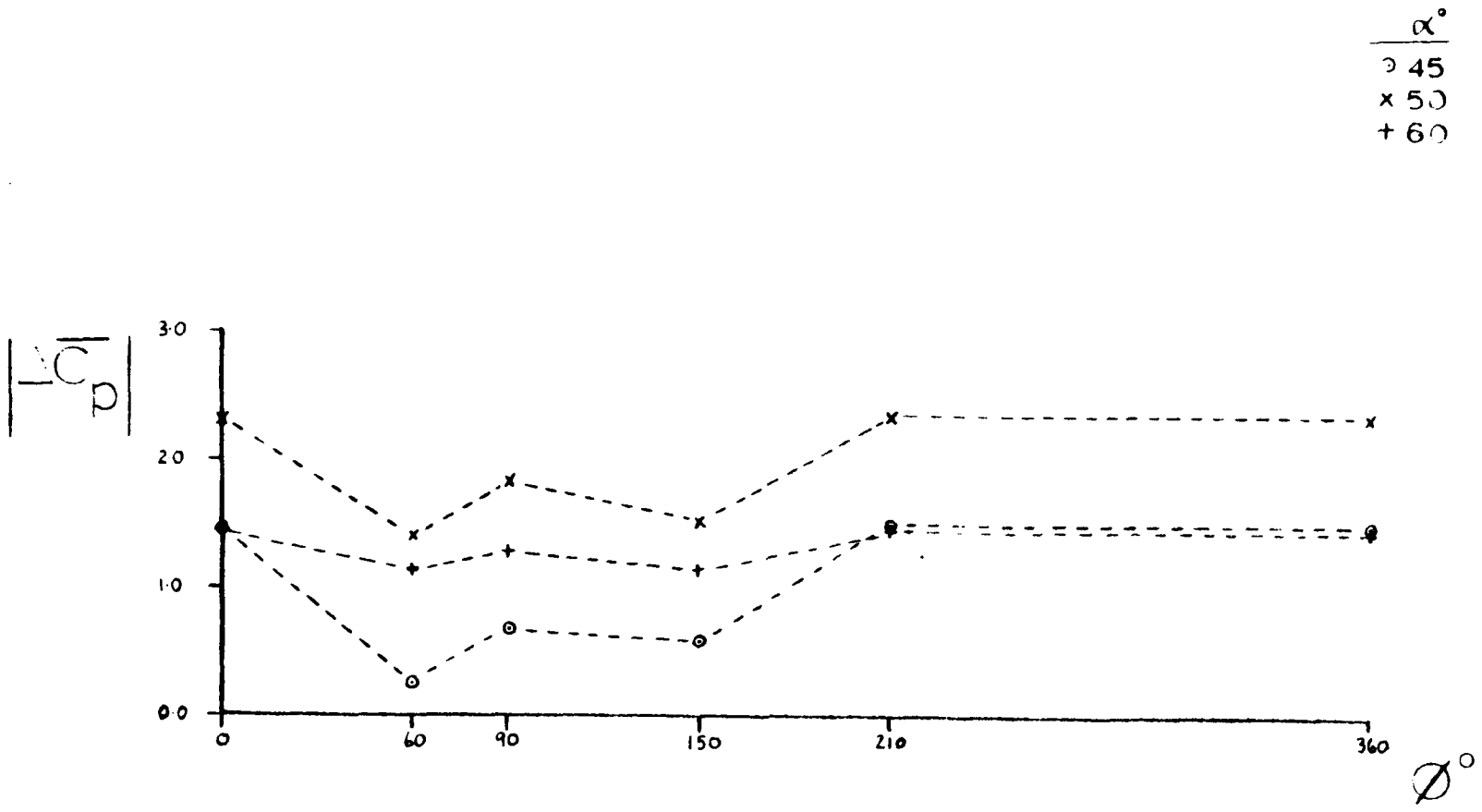

FIGURE 9 $|\Delta C_p|$ vs ROLL ANGLE AT VARIOUS INCIDENCES, Re = 0·5E5, x/D = 5, 38mm MODEL

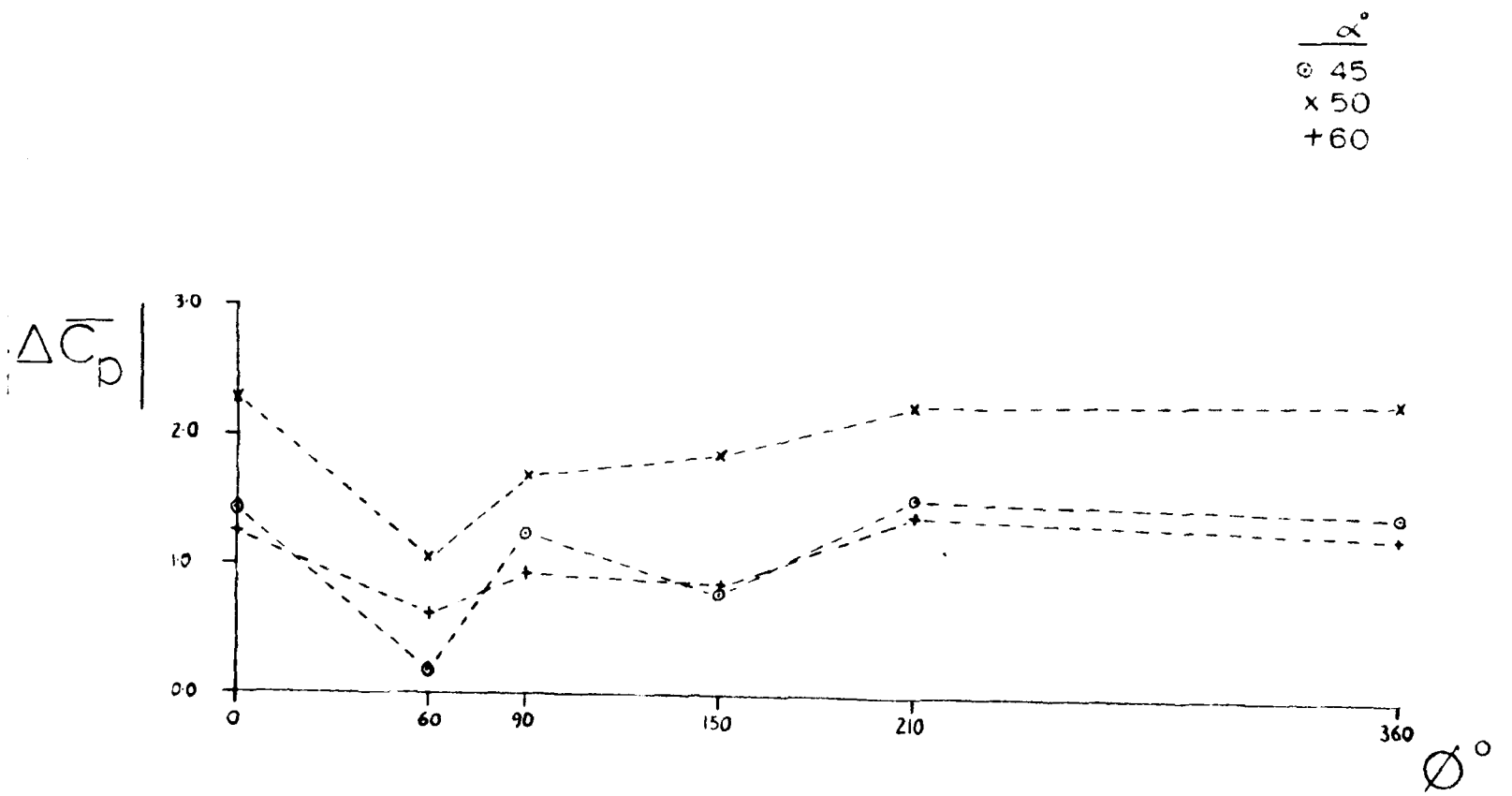

FIGURE 10 $|\Delta\overline{C_p}|$ vs ROLL ANGLE AT VARIOUS INCIDENCES, Re = 1·0E5, x/D = 5, 38 mm MODEL

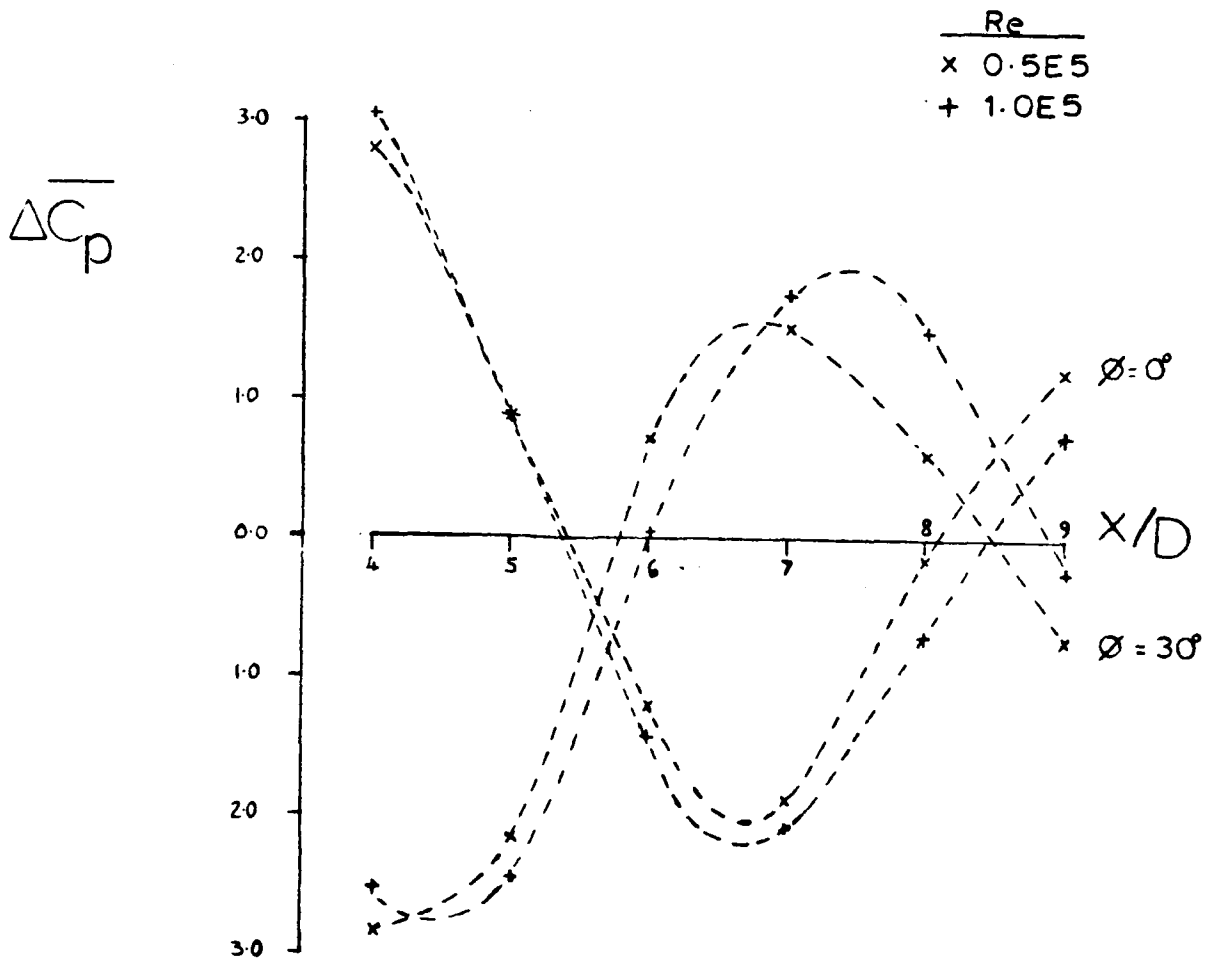

FIGURE 11 $\overline{\Delta C_p}$ DISTRIBUTION FROM TRANSIENT PRESSURE RECORDING TESTS

$\alpha = 50°$

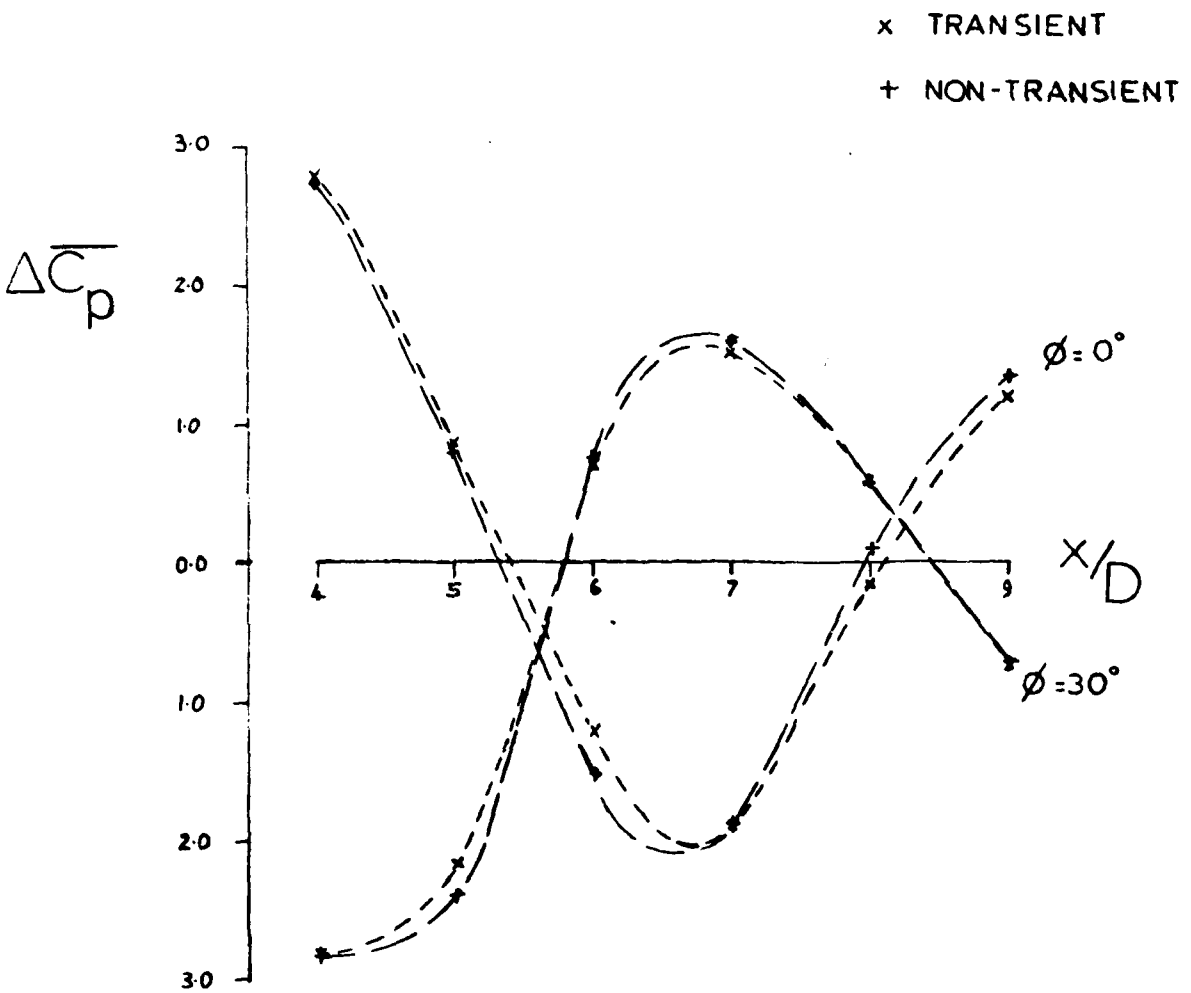

FIGURE 12 COMPARISON OF TEST METHODS, $\Delta\overline{C_p}$ DISTRIBUTION. Re=0.5E5, $\alpha = 50°$

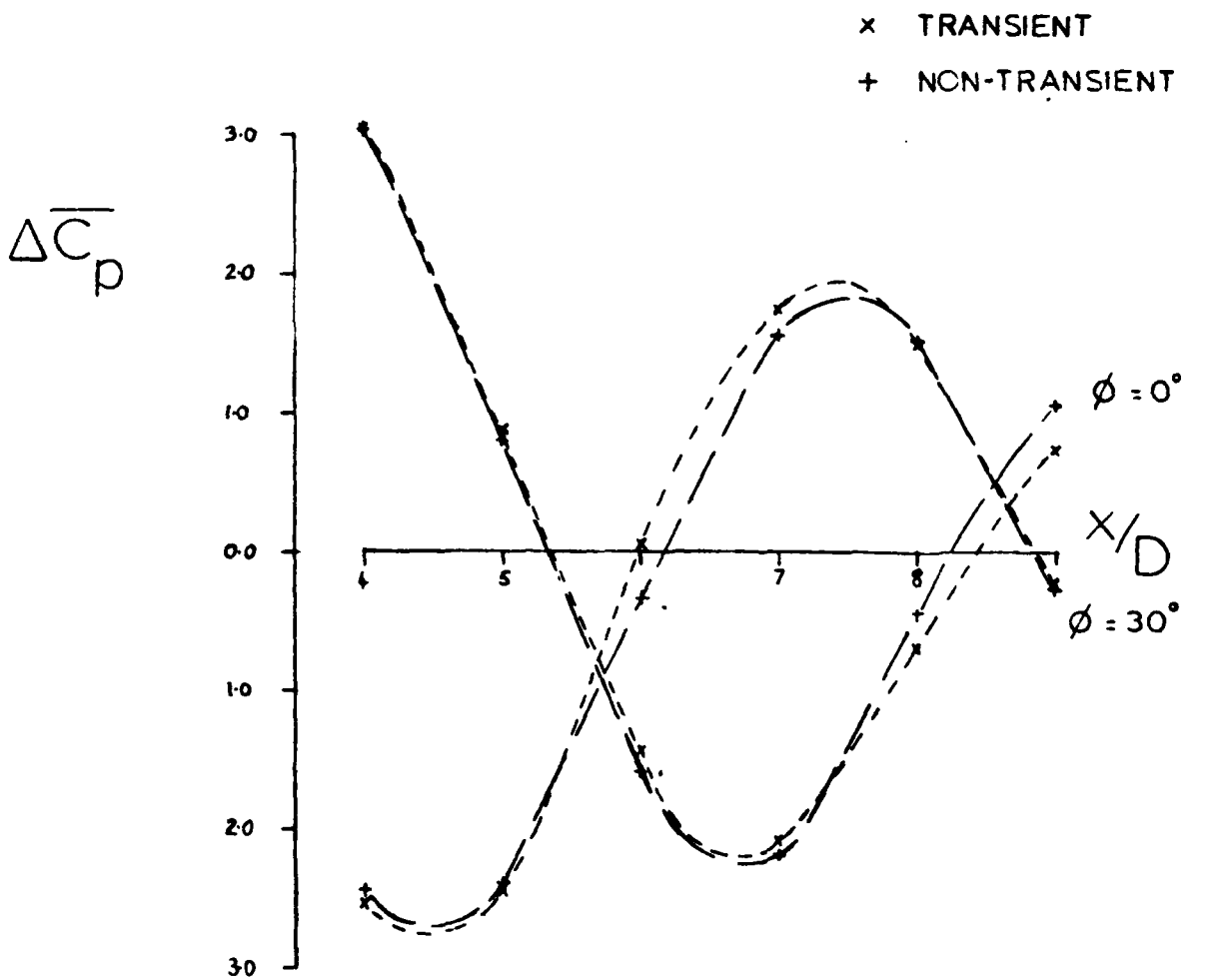

FIGURE 13 COMPARISON OF TEST METHODS, $\Delta\overline{C_p}$ DISTRIBUTION. Re=1·0E5, α=50°

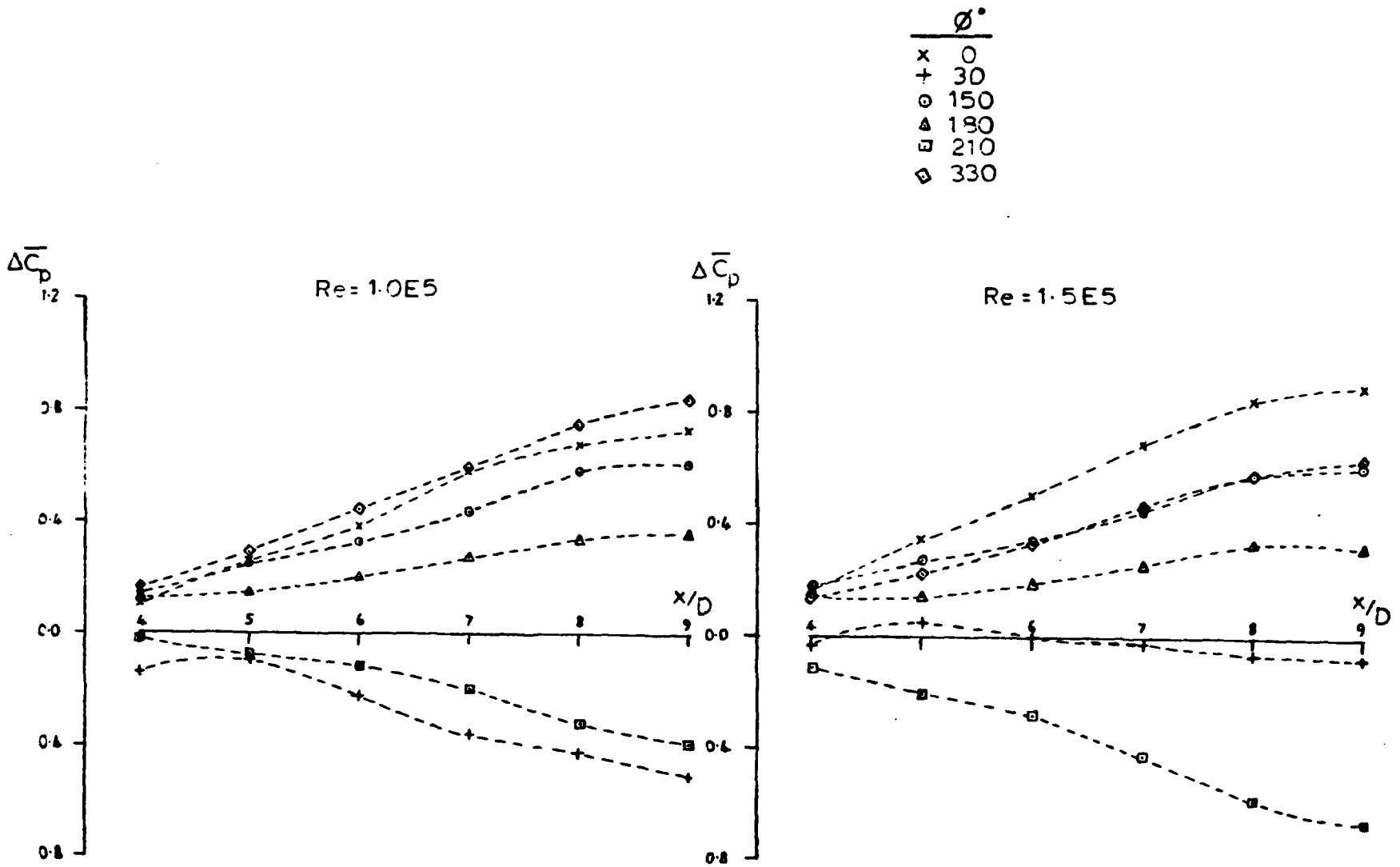

FIGURE 14 $\Delta \bar{C}_p$ DISTRIBUTION $\alpha = 30°$

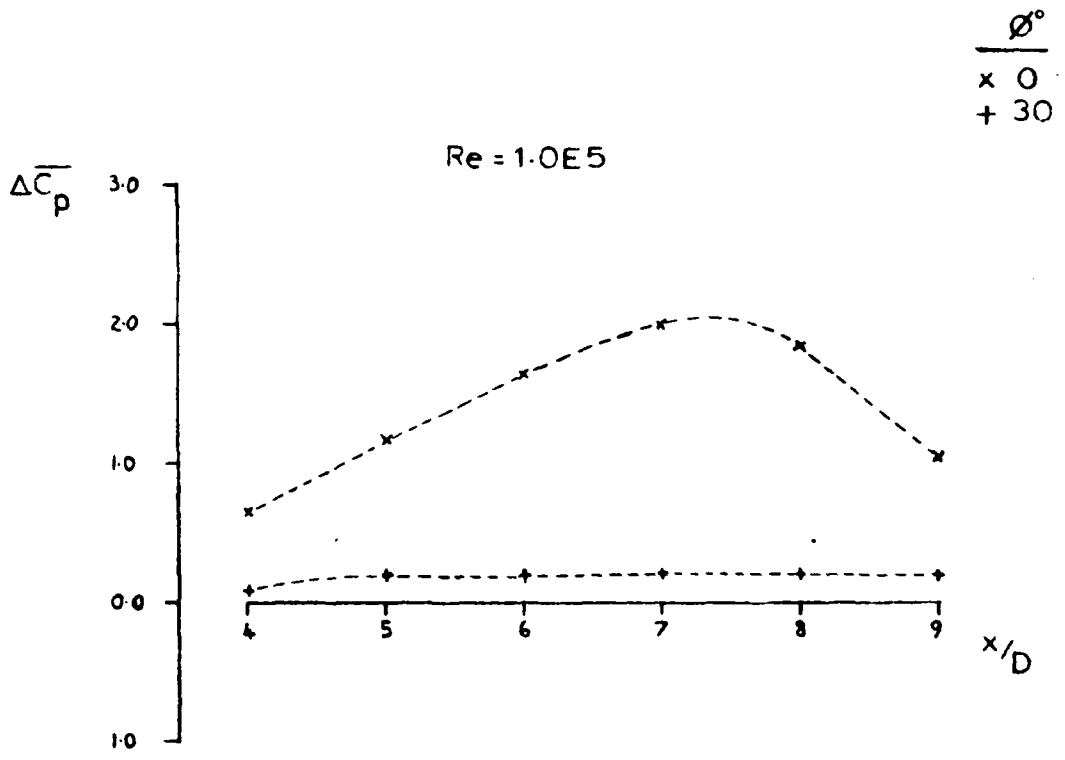

FIGURE 15 $\Delta\overline{C_p}$ DISTRIBUTION $\alpha = 35°$

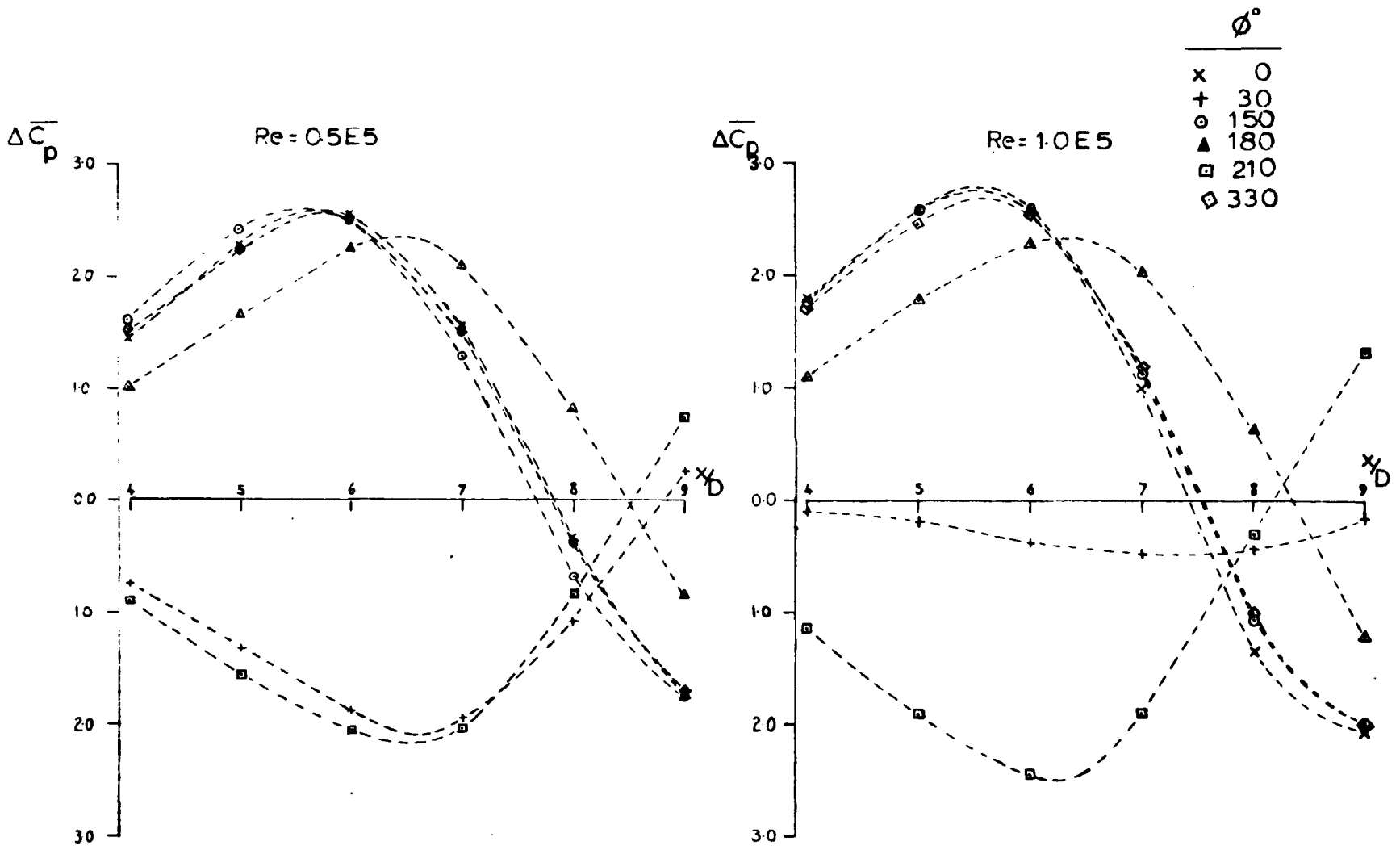

FIGURE 16 $\Delta \overline{C_p}$ DISTRIBUTION $\alpha = 40°$

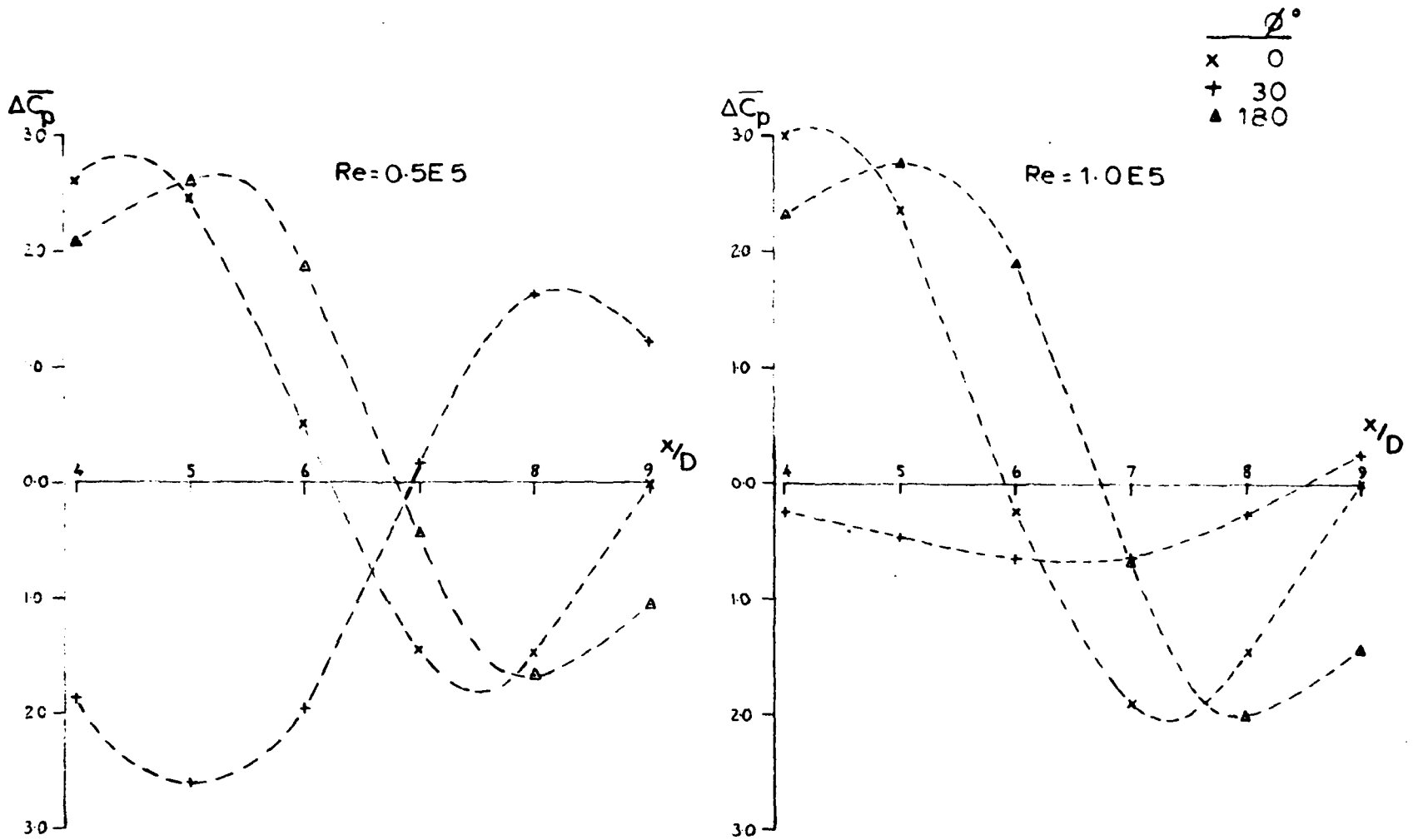

FIGURE 17 $\Delta\bar{C}_p$ DISTRIBUTION $\alpha = 45°$

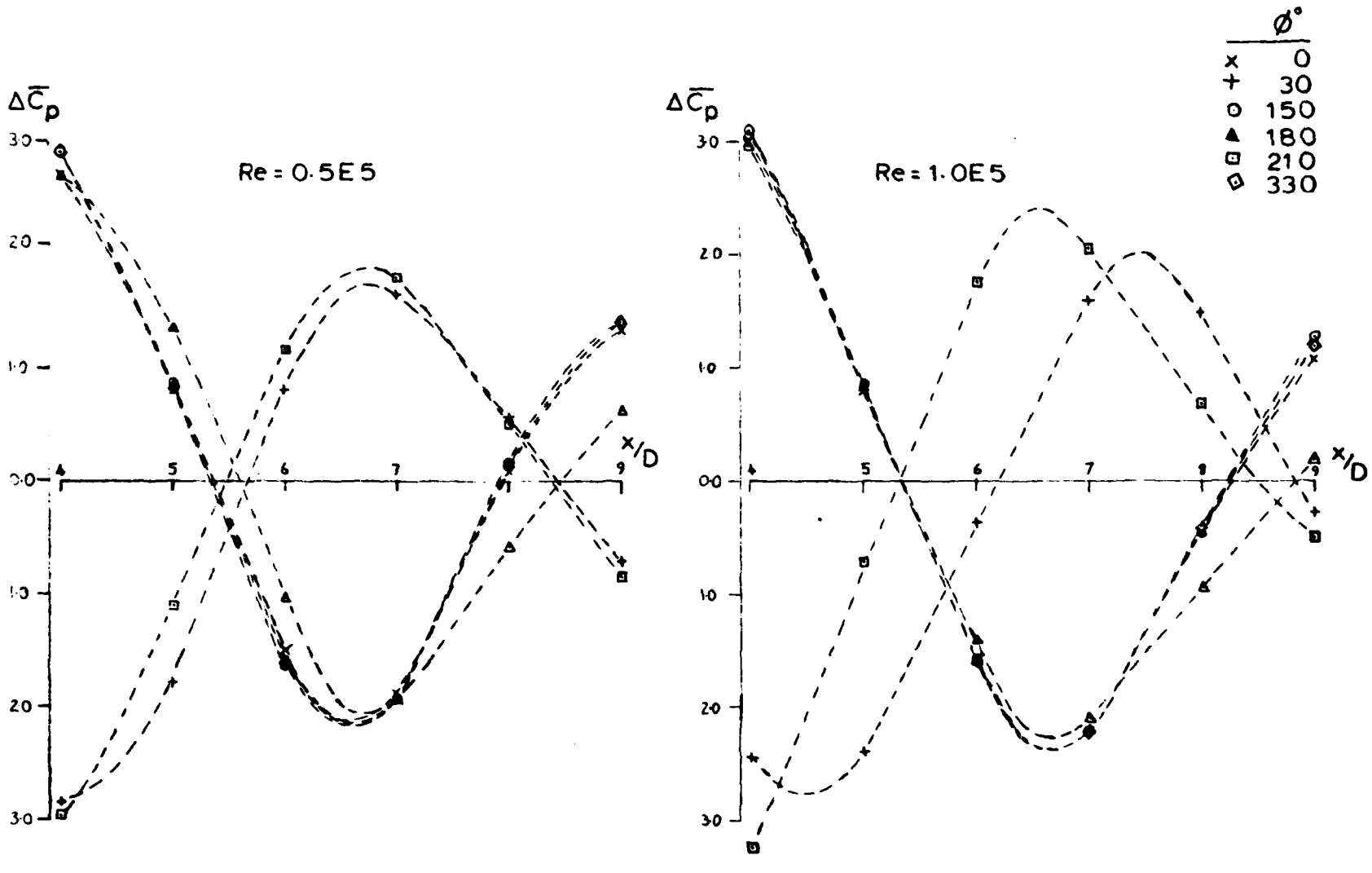

FIGURE 18 $\Delta\overline{C_p}$ DISTRIBUTION $\alpha = 50°$

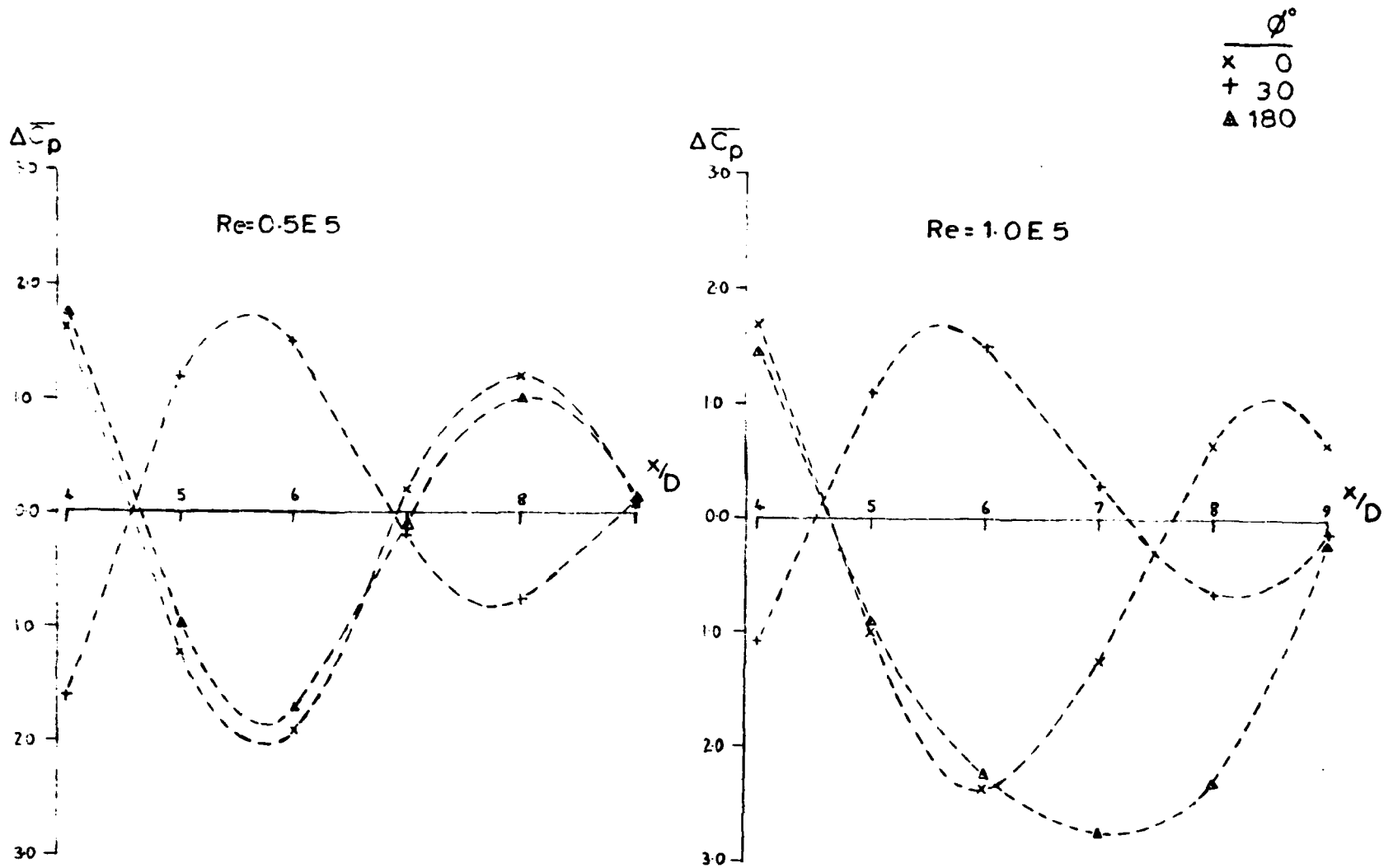

FIGURE 19 $\Delta \bar{C}_p$ DISTRIBUTION $\alpha = 55°$

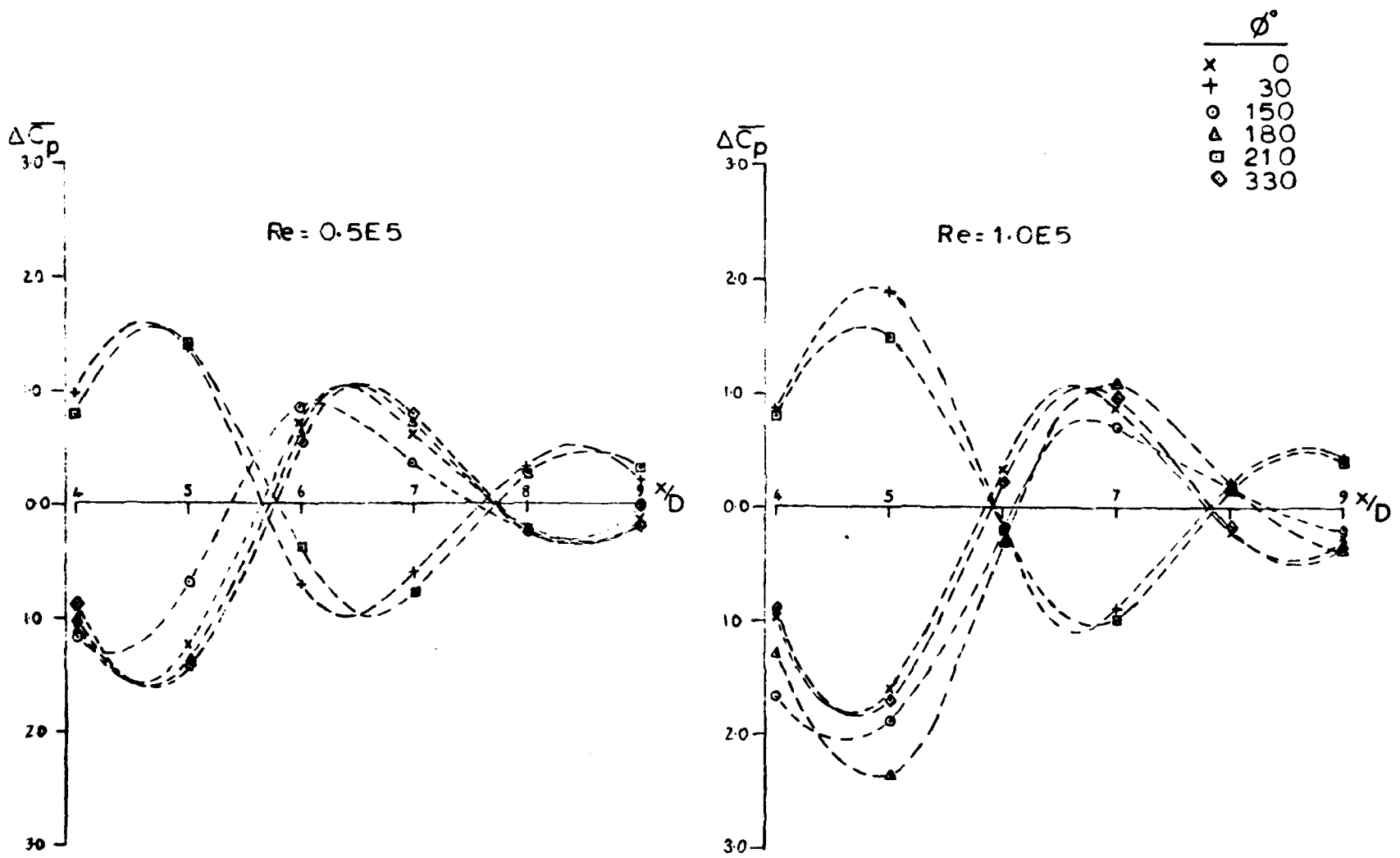

FIGURE 20 $\Delta\bar{C}_p$ DISTRIBUTION $\alpha = 60°$

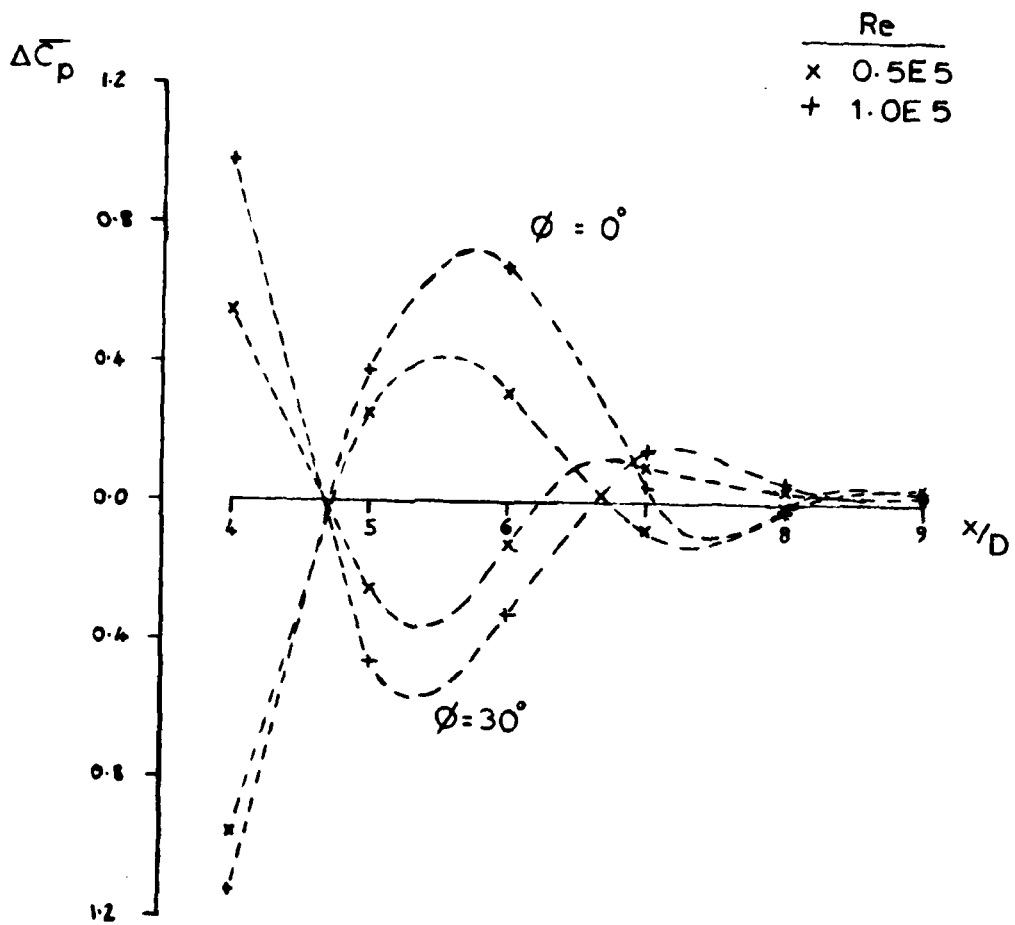

FIGURE 21 $\Delta\overline{C_p}$ DISTRIBUTION $\alpha = 65°$

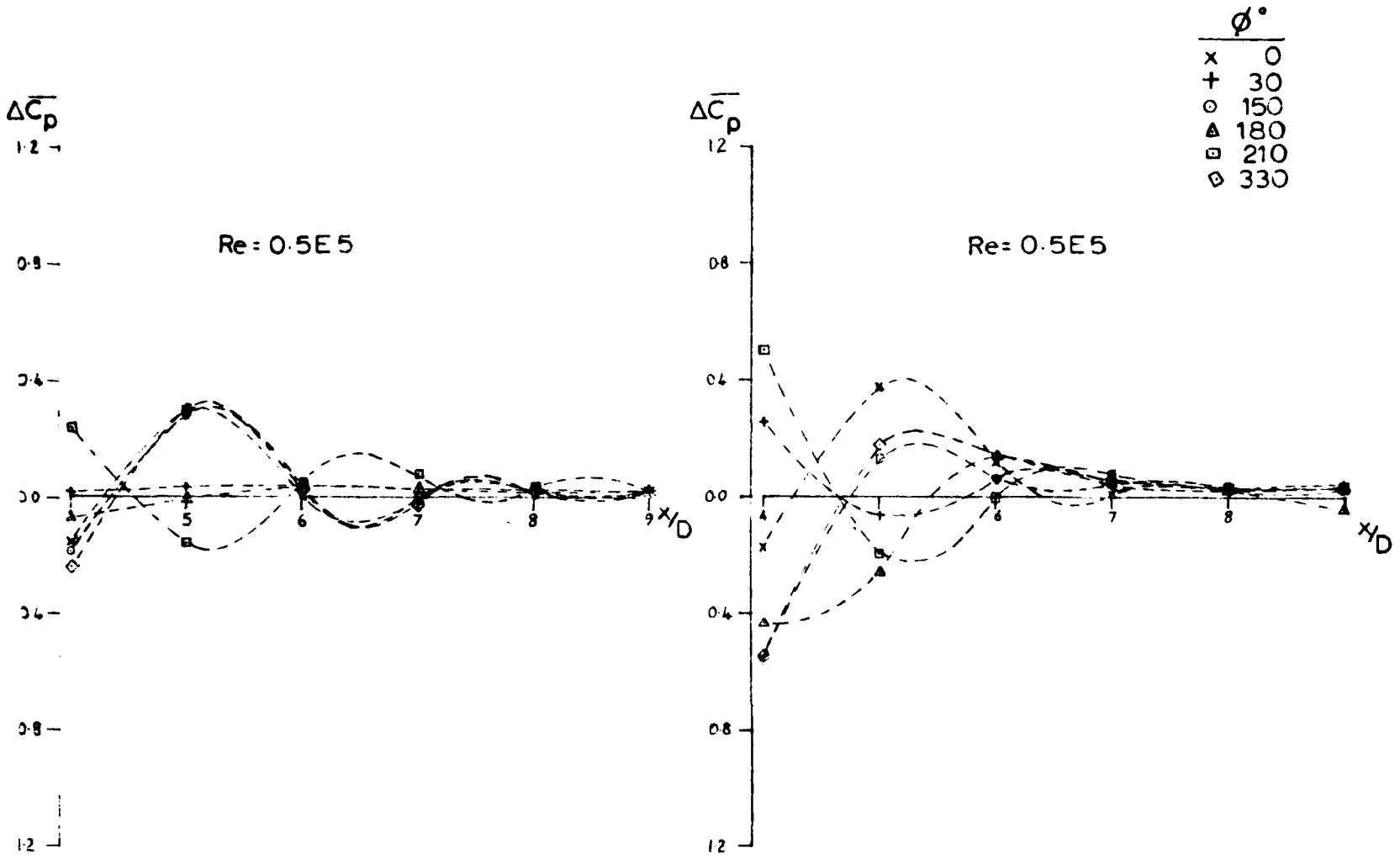

FIGURE 22 $\Delta\overline{C_p}$ DISTRIBUTION $\alpha = 70^\circ$

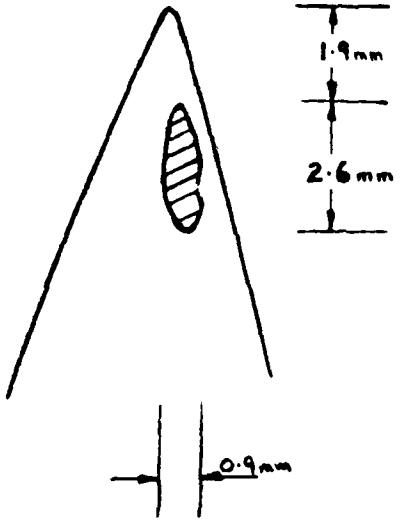

DIMENSIONS OF DENT
ON MODEL NOSE TIP

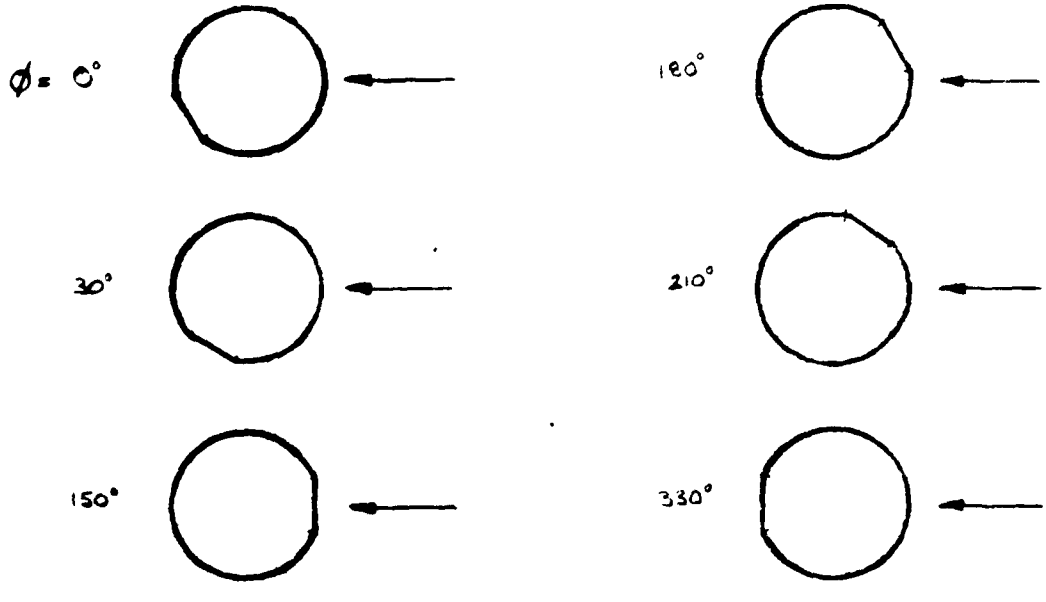

DENT ORIENTATION AT VARIOUS ROLL ANGLES RELATIVE TO FREESTREAM CROSSFLOW

FIGURE 23

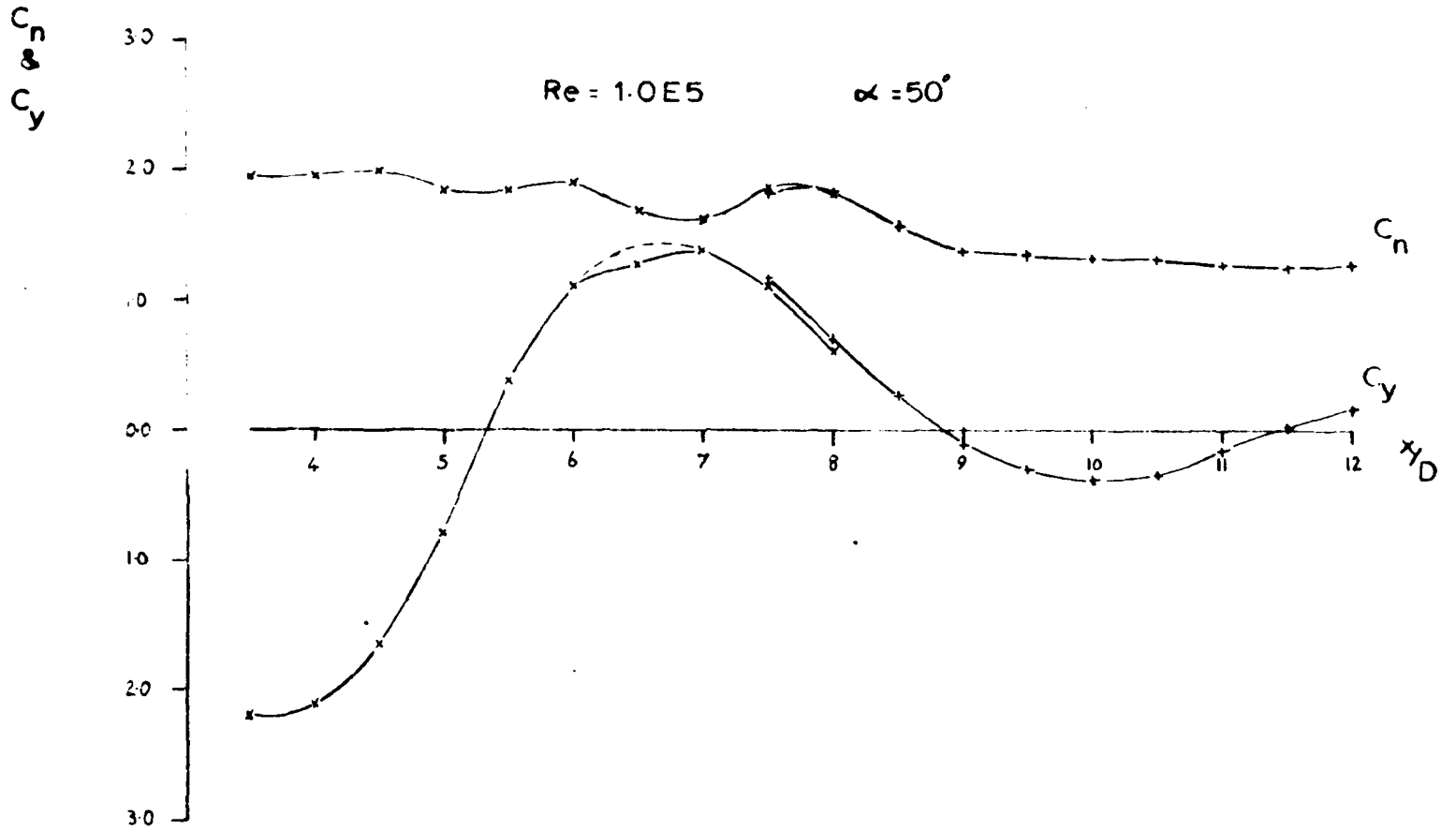

FIGURE 24 FORCE DISTRIBUTION, OLD NOSE, $\phi = 0^\circ$

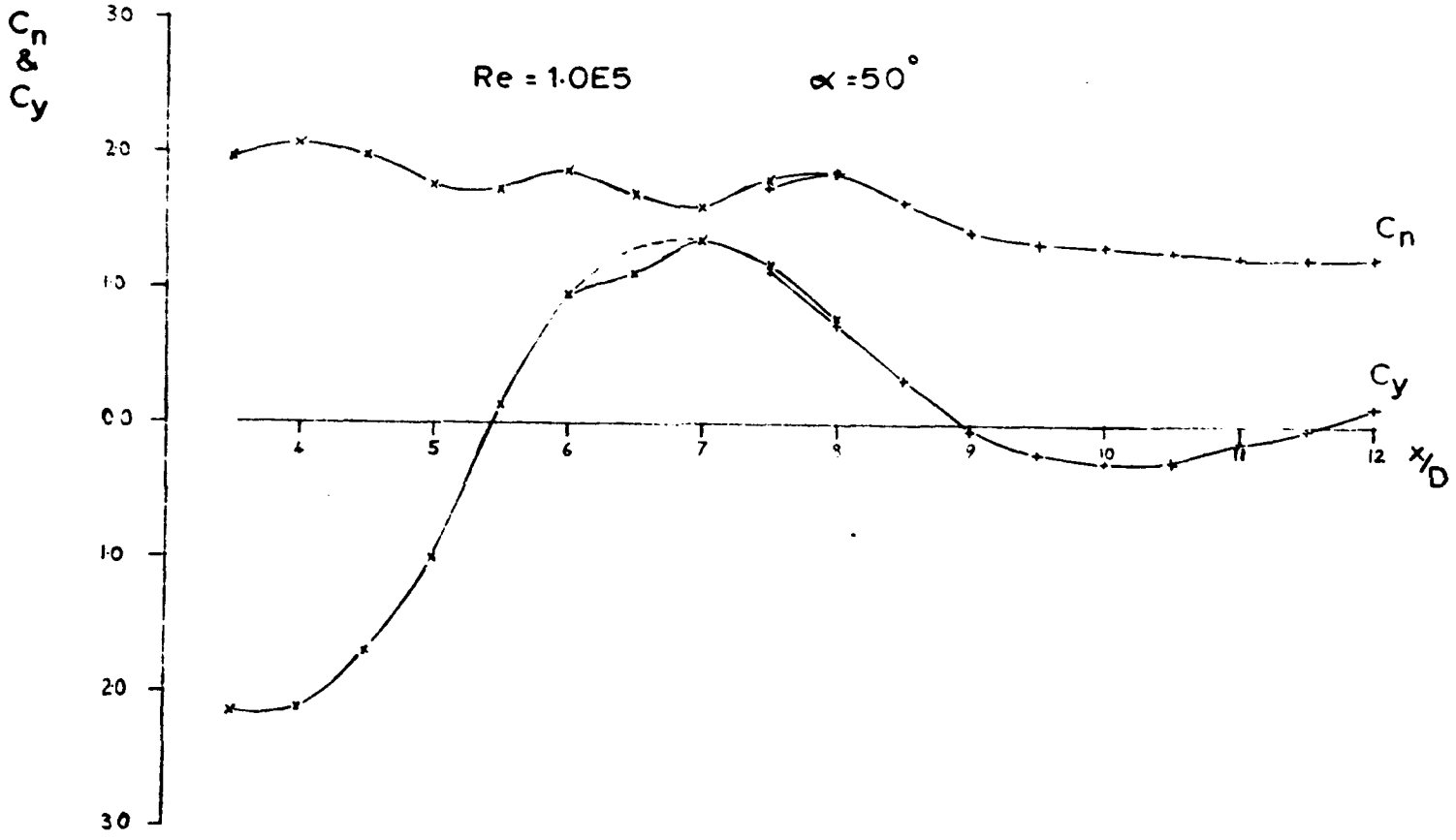

FIGURE 25 FORCE DISTRIBUTION , STEEL NOSE, $\phi = 0^\circ$

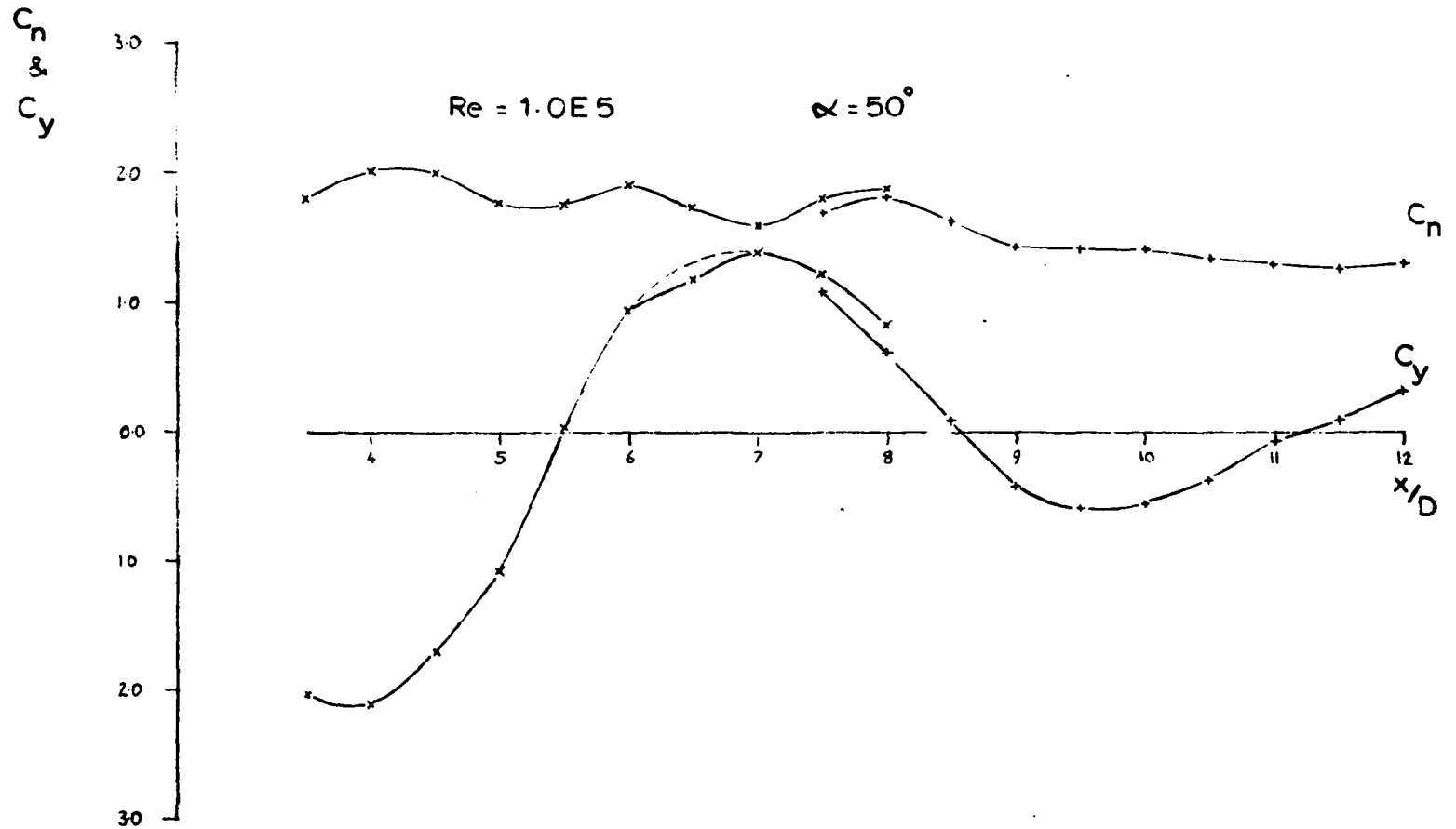

FIGURE 26 FORCE DISTRIBUTION , OLD NOSE, $\phi = 30^\circ$

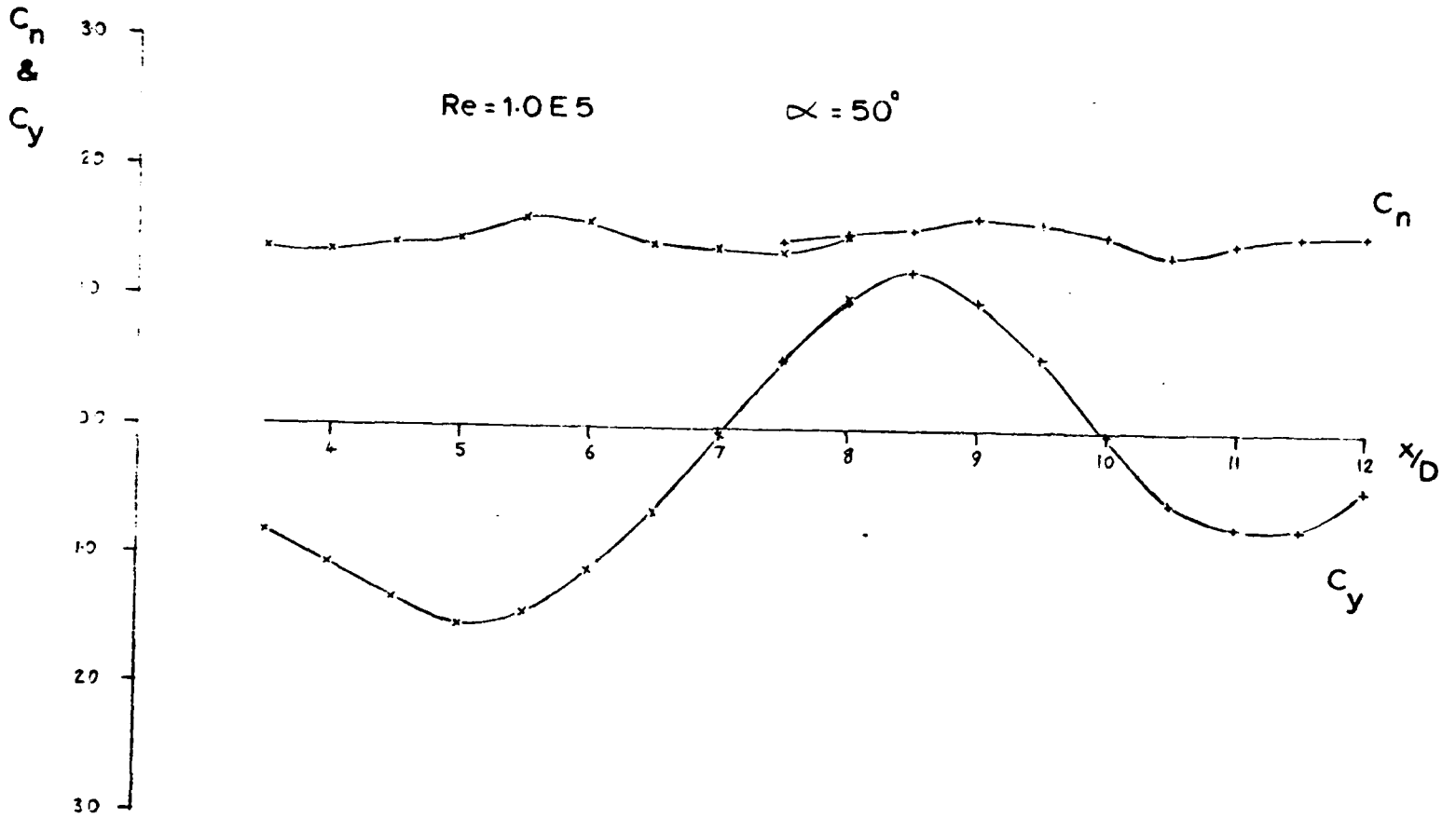

FIGURE 27 FORCE DISTRIBUTION, STEEL NOSE, $\phi = 30°$

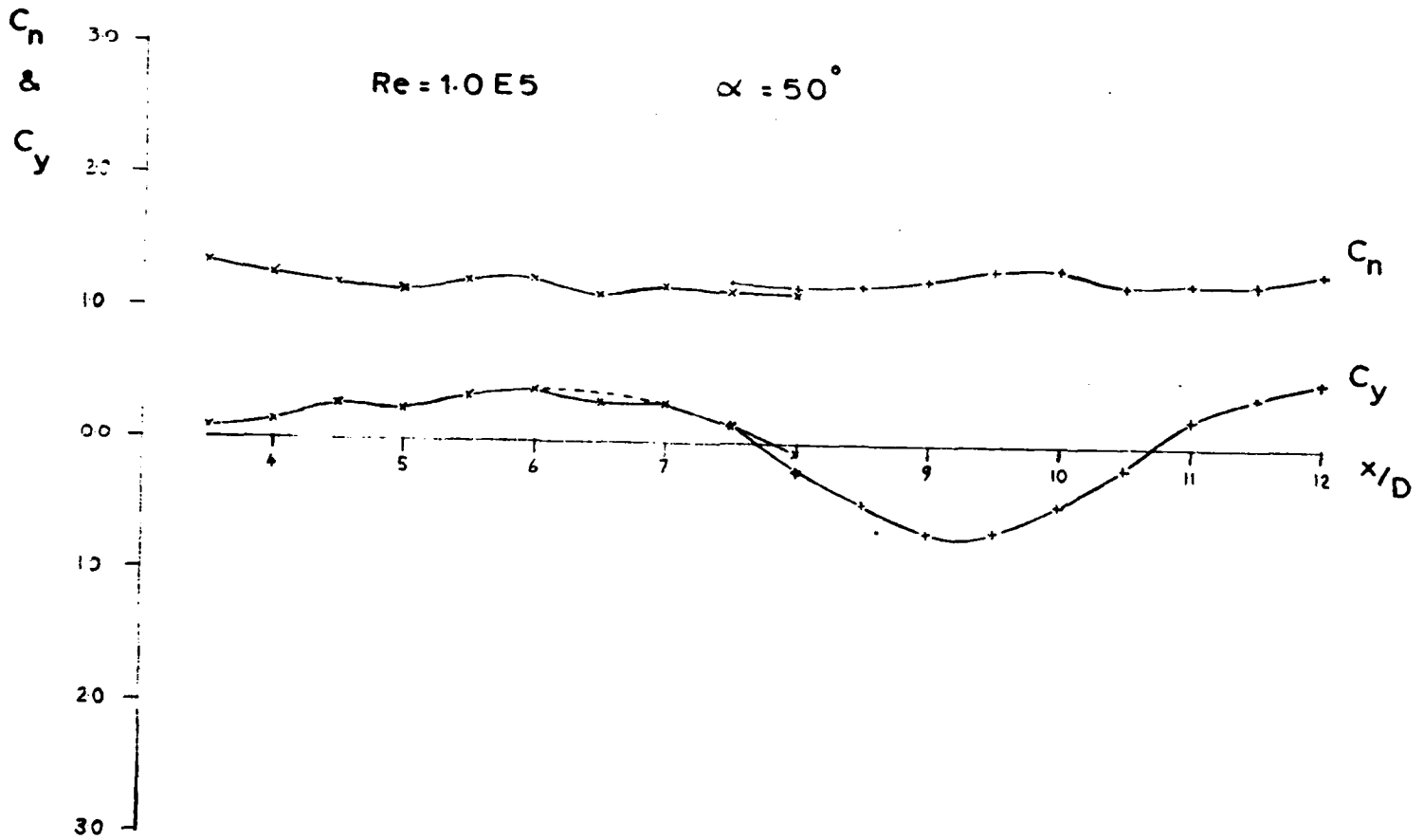

FIGURE 28 FORCE DISTRIBUTION , OLD NOSE, $\phi = 60^\circ$

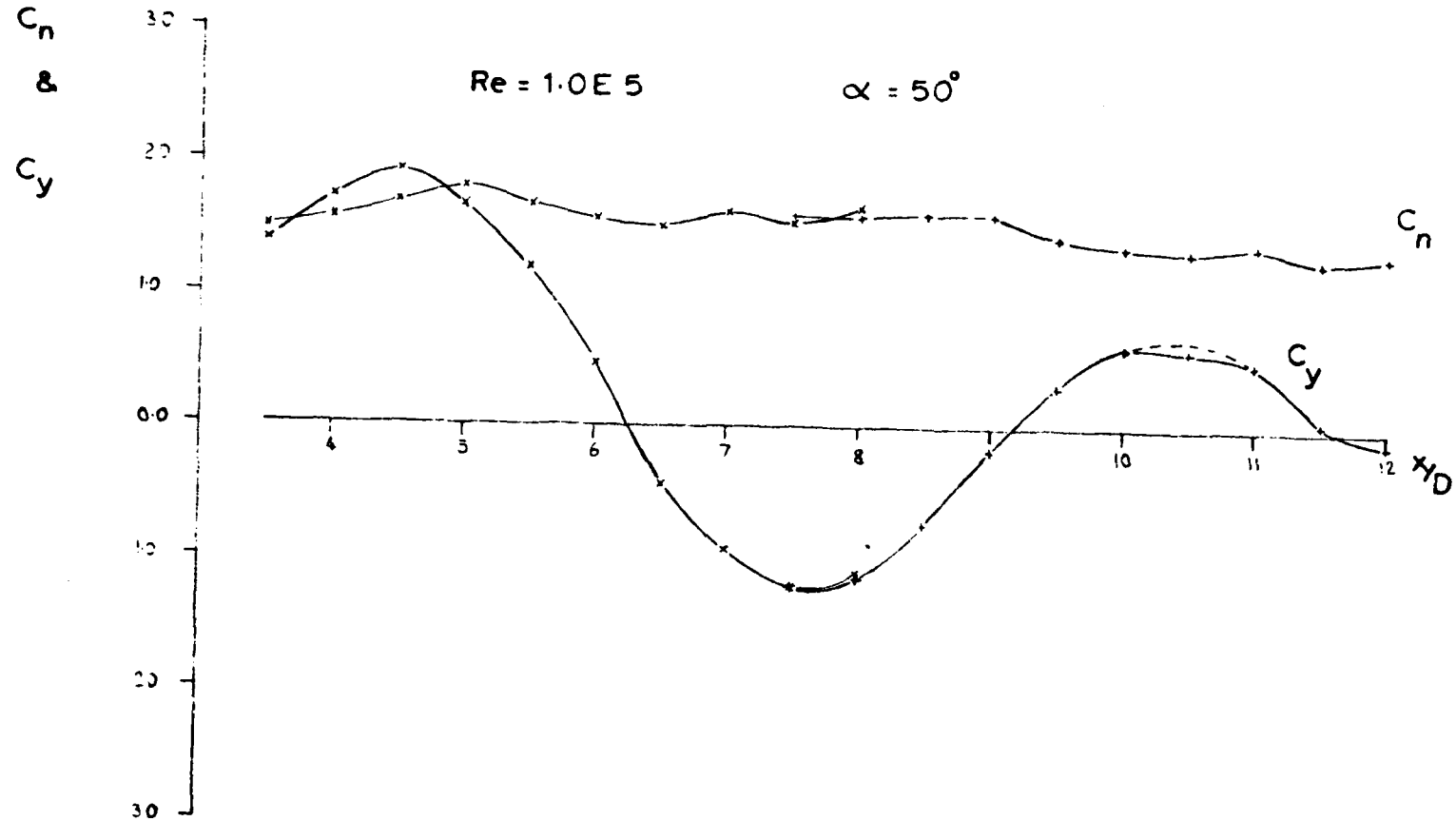

FIGURE 29 FORCE DISTRIBUTION , STEEL NOSE , ϕ = 60°

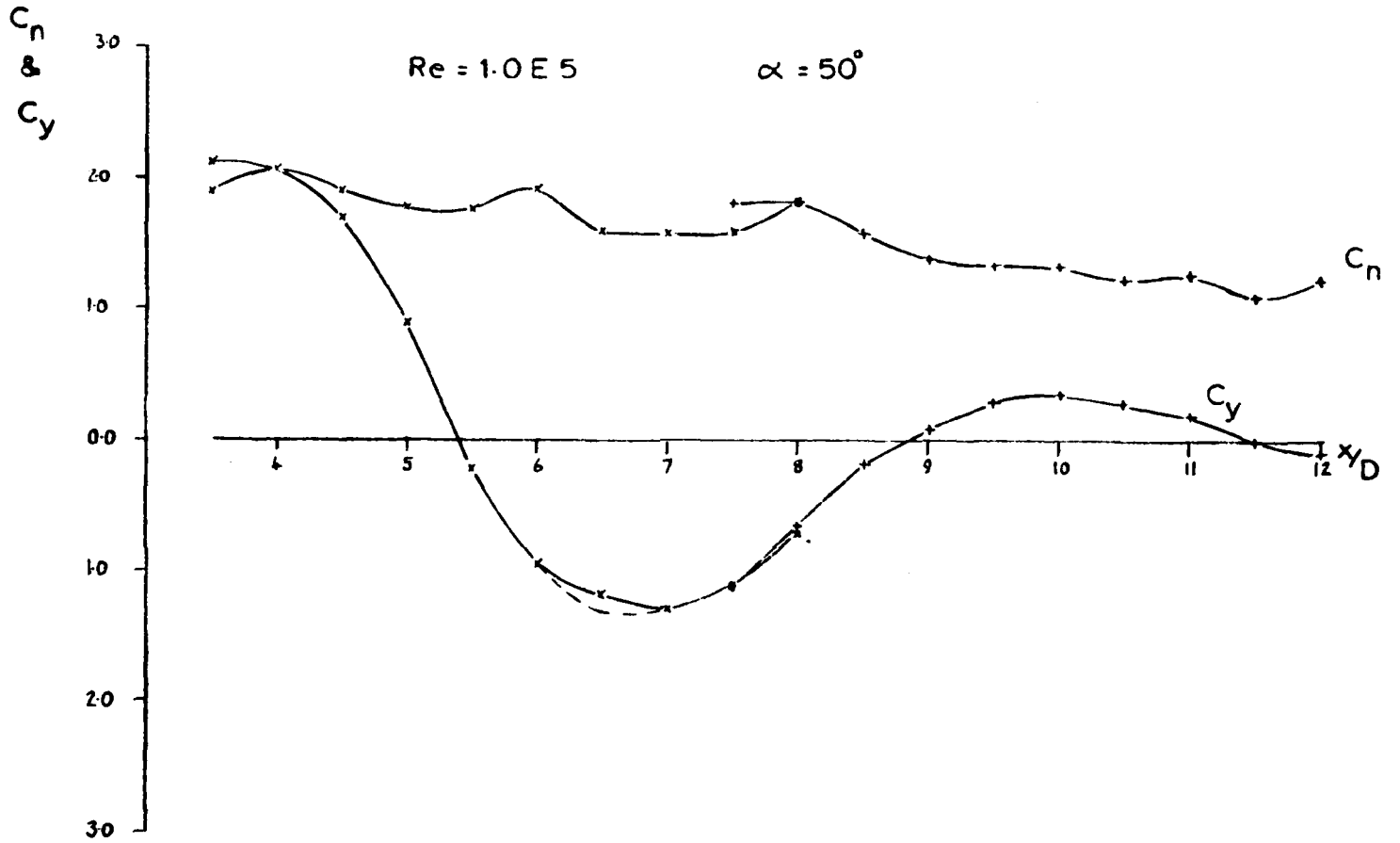

FIGURE 30 FORCE DISTRIBUTION , OLD NOSE, ϕ = 90°

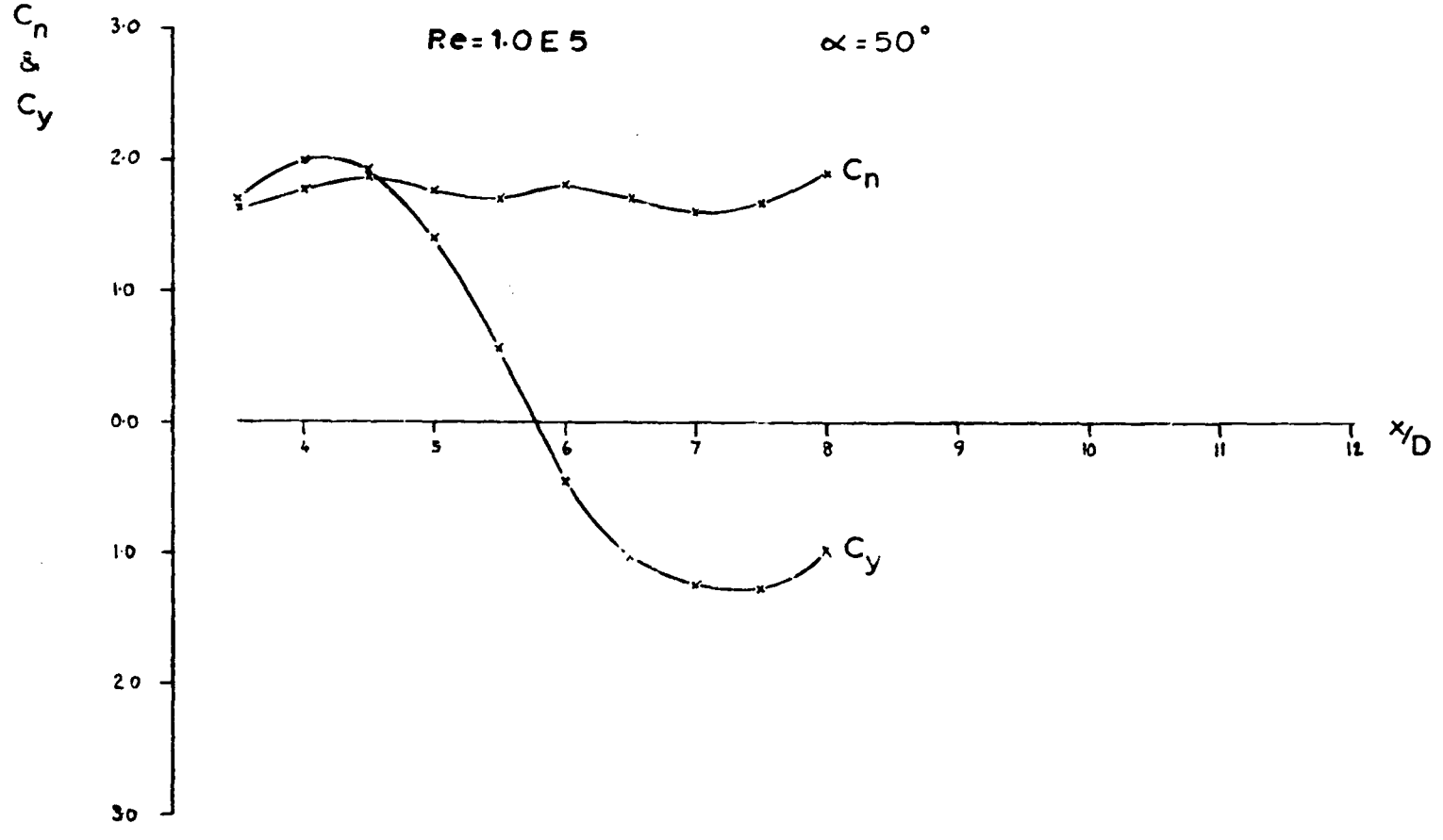

FIGURE 31 FORCE DISTRIBUTION , STEEL NOSE, $\phi = 90°$

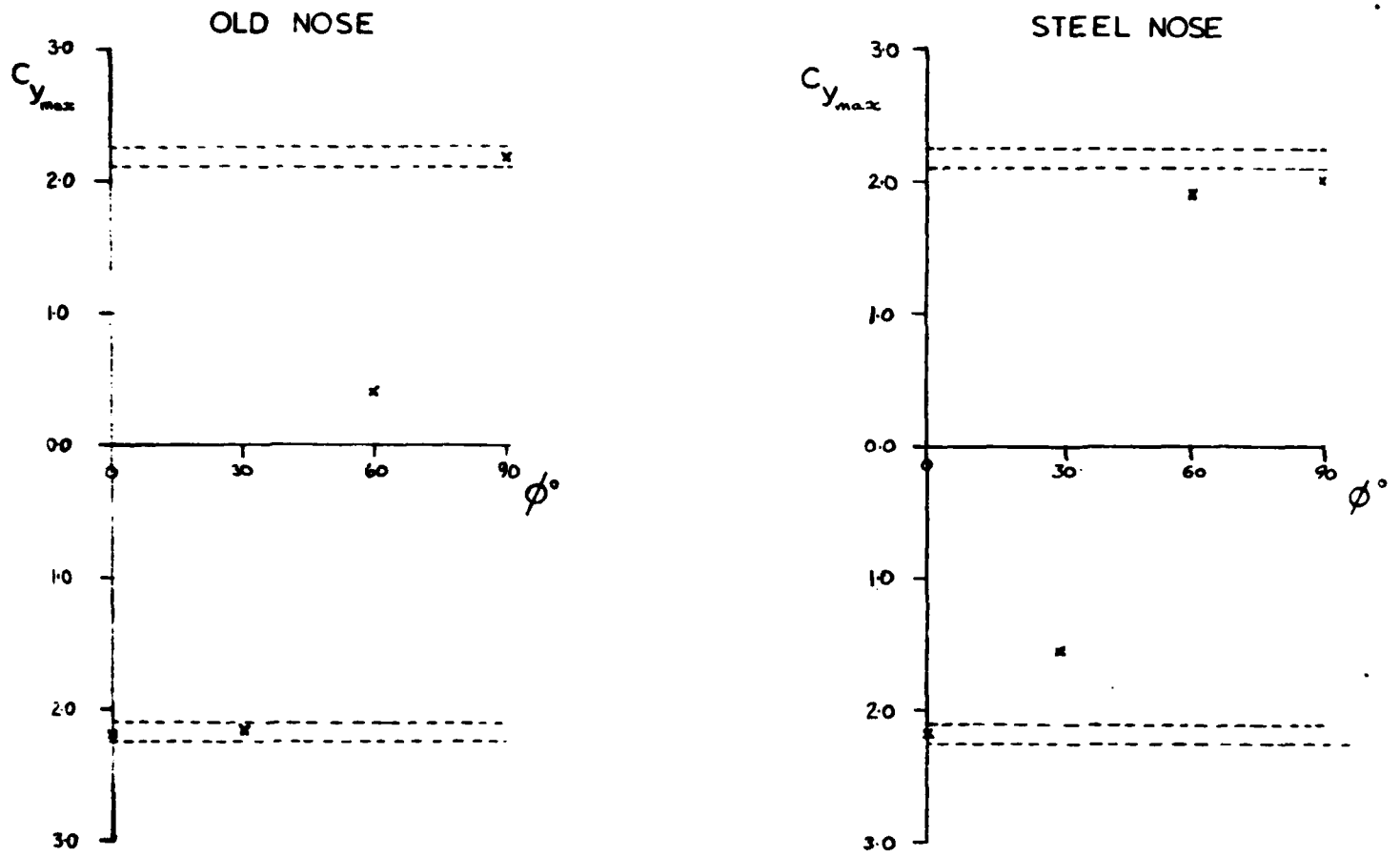

FIGURE 32 VARIATION OF $C_{y_{max}}$ WITH ROLL ANGLE

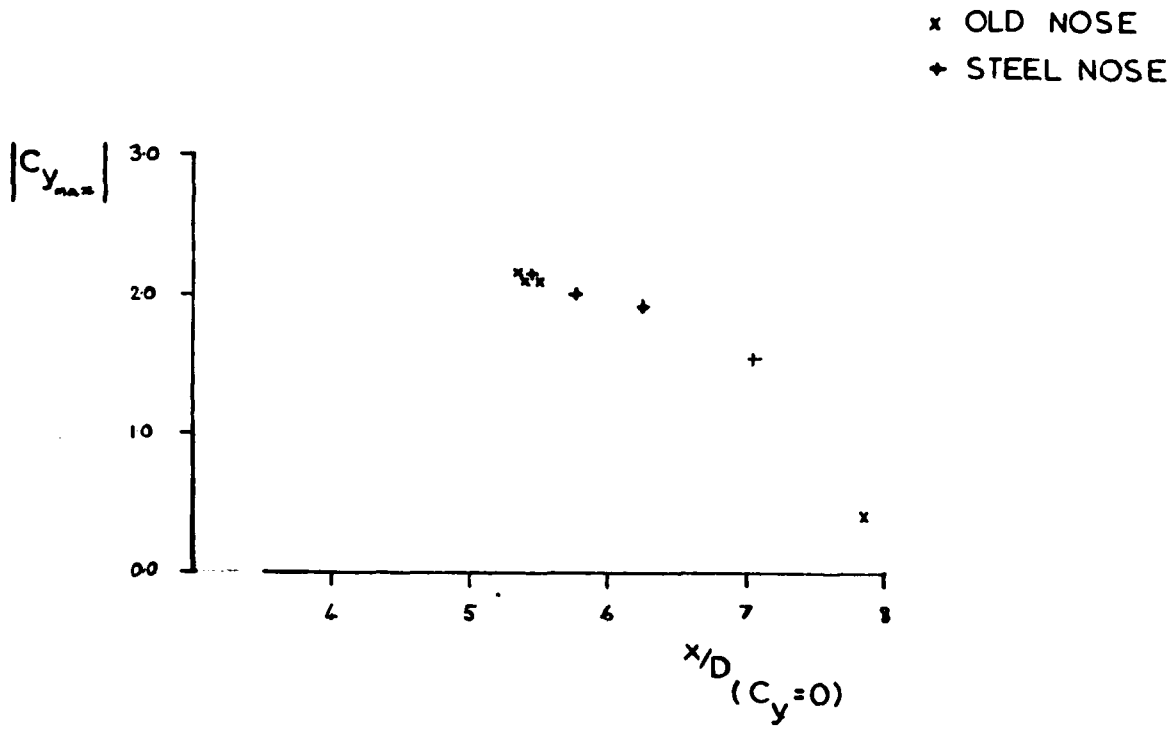

FIGURE 33 $C_{y_{max}}$ versus C_y DISTRIBUTION NODE POINT

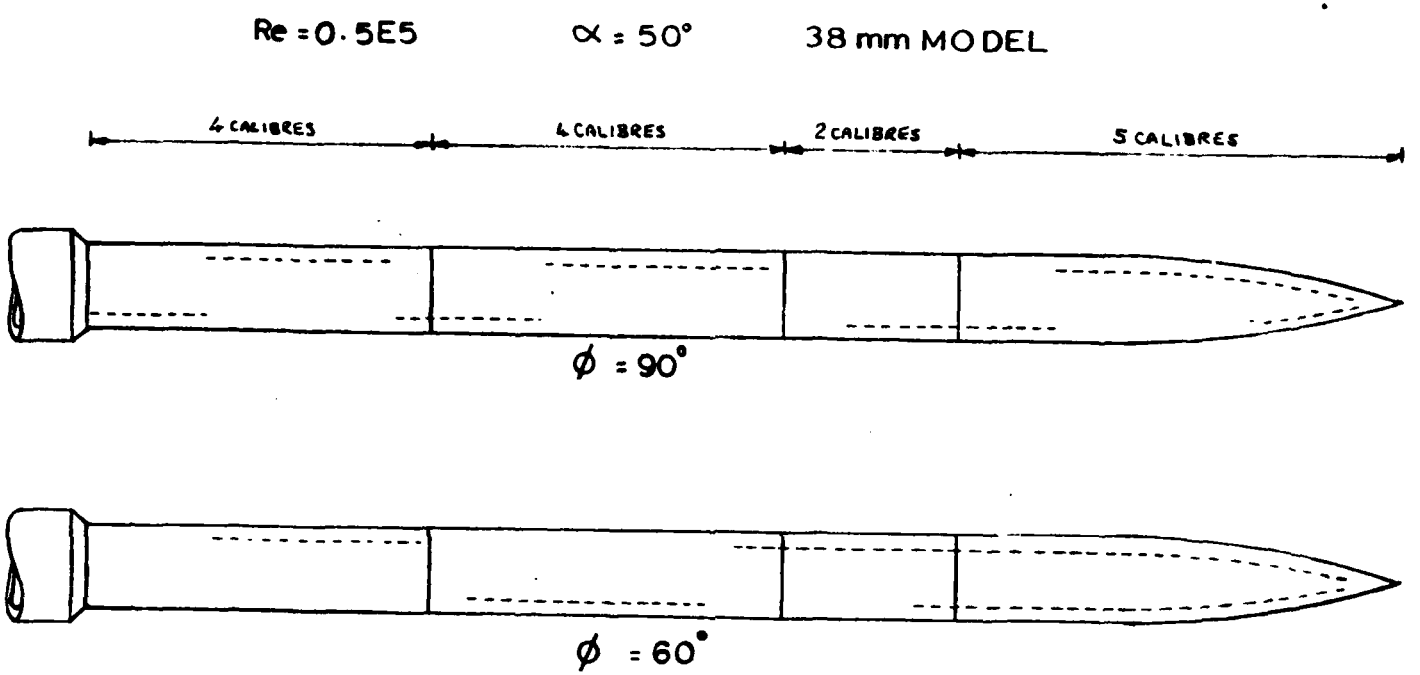

FIGURE 34 SKETCH OF ATTACHED VORTEX POSITIONS FROM WOOL TUFT PROBE